9
Some Exact Solutions

The Navier–Stokes equations are the most famous and perhaps the most important equations in fluid mechanics. In biofluid mechanics, these equations can be used to compute the flow of air within the airways, the flow of blood in large vessels at sufficiently high shear rates, the flow of urine from the bladder, the flow of crystalloid perfusates in in vitro experiments, and so on. Because few analytical solutions are available, one must often resort to numerical methods to solve these important equations. Nonetheless, in this chapter, we will consider five important analytical solutions to the Navier–Stokes equations.

Recall from Chap. 8 that the two governing differential equations for an incompressible, Newtonian flow are

$$\nabla \cdot \boldsymbol{v} = 0 \tag{9.1}$$

which enforces the balance of mass, and

$$-\nabla p + \mu \nabla^2 \boldsymbol{v} + \rho \boldsymbol{g} = \rho \left[\frac{\partial \boldsymbol{v}}{\partial t} + (\boldsymbol{v} \cdot \nabla) \boldsymbol{v} \right], \tag{9.2}$$

which enforces the balance of linear momentum. Again, $\boldsymbol{v}$ is the velocity, p is the fluid pressure, μ is the viscosity, ρ is the mass density, and $\boldsymbol{g}$ is the body force vector per unit mass; Eq. (9.2) is the so-called incompressible Navier–Stokes equation.

Here, we will consider three classes of incompressible flows: (1) in vivo flows, (2) in vitro flows in experiments that are useful in cell biology, and (3) in vitro flows that can be used to quantify the viscous behavior of particular Newtonian fluids. With regard to the first class of flows, note that several complicating conditions exist in large arteries and large airways, such as the

J.D. Humphrey, S.L. O'Rourke, *An Introduction to Biomechanics*,
DOI 10.1007/978-1-4939-2623-7_9

pulsatility (i.e., unsteadiness) of the pressures as well as the distensibility of the tubes. These perhaps seemingly simple characteristics add tremendous complexity to the formulation and solution of the associated initial-boundary value problems. In particular, computing flows within distensible tubes necessitates the solution of coupled solid–fluid mechanics problems. Such solutions are the topic of current research and generally beyond the scope of an introductory text; we address them only briefly in Chap. 11. Fortunately, there are still many in vivo situations for which it may be reasonable to assume a steady flow within a "rigid" tube. For example, some left ventricular-assist devices output a steady flow to the aorta, and aortic stiffness allows only small changes in radius in this situation. Likewise, venous flows are nearly steady and there is little change in the radius of the vessel at a given location. If we integrate over time (i.e., over the cardiac cycle), we also find that the time-averaged shear stress on the arterial wall is approximated reasonably well in some situations by the steady-flow solution. Hence, we will carefully consider a number of solutions for steady flow. Finally, we must remember that blood only exhibits a Newtonian response at high shear rates. There is a need, therefore, to consider non-Newtonian behavior as well, which we do briefly in the last section of this chapter.

9.1 Flow Between Parallel Flat Plates

9.1.1 Biological Motivation

Cellular function is so complex that it was realized many years ago that it can be very useful to study the response of isolated cells to well-controlled stimuli. For example, the endothelial cells that line the inner (luminal) surface of the vasculature are sensitive to fluid-induced shear stresses. Muscular arteries appear to vasoconstrict or vasodilate, via smooth muscle contraction and relaxation, so as to maintain the wall shear stress τ_w nearly constant. This vasomotion is controlled, in part, by endothelial production of vasoactive molecules such as the vasodilators nitric oxide (NO) and prostacyclin (PGI_2) and the vasoconstrictors endothelin-1 (ET-1) and thromboxane (TXA_2). In general, as τ_w is increased by an increased flow (e.g., during exercise), the endothelium produces more vasodilators to increase the lumen and thereby restore the wall shear stress to its normal value; the converse occurs when τ_w is decreased by a decreased flow (e.g., due to a sedentary lifestyle). See Fig. 9.1. Of course, many conditions can alter blood flow, including changes during pregnancy due to the presence of placental flow, changes in luminal geometry due to atherosclerosis, and the surgical creation of an arterio-venous fistula (or shunt) in kidney dialysis patients. An important research goal is to correlate the endothelial production of these various molecules with alterations in flow-induced shear stresses. To do this, *we need solutions of initial-boundary value problems that represent convenient experimental situations*, one of which is flow between rigid parallel plates.

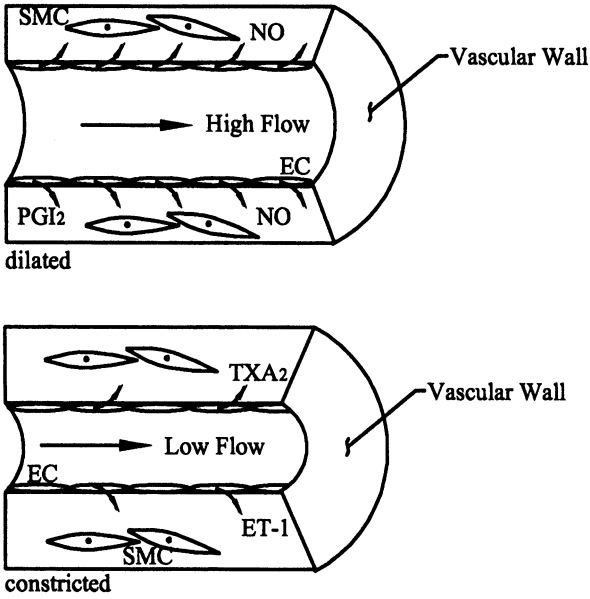

FIGURE 9.1 Schema showing the lumen and section of a vascular wall in response to two different altered stimuli: a sustained increase in flow, which increases the lumen, and a sustained decrease in flow, which decreases the lumen. It is not uncommon, for example, for marathon runners to have significantly larger iliac arteries due to the consistent elevation of blood flow because of training. It is thought that such changes in lumen maintain the wall shear stress at its homeostatic value. Albeit not shown, a sustained increase in pressure results in an increase in the thickness of the vascular wall. It is thought that this response maintains the circumferential wall stress near its homeostatic value.

9.1.2 Mathematical Formulation

A useful in vitro experiment is to culture a monolayer of endothelial cells on one of two parallel flat plates and then to subject the system to a pressure-driven flow (Fig. 9.2). Although the monolayer has a cobblestone or undulating appearance on a microscale, the cells being thicker in the region of their nucleus, we shall assume for our purposes that both the cell layer and the opposing plate are flat. This is a reasonable assumption when the variation in cell height is on the order of micrometers and the spacing between the plates is on the order of millimeters or centimeters. Moreover, we will assume that the flow is steady, incompressible, and Newtonian, thus allowing us to formulate the experimental boundary value problem within the context of an exact solution of the Navier–Stokes equation. Indeed, because we are the ones who design the experiment, we can ensure the use of a fluid that exhibits an

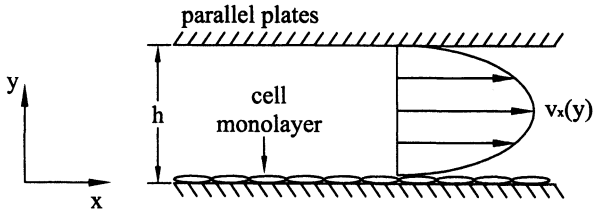

FIGURE 9.2 Steady flow of a Newtonian fluid (e.g., culture media) between two rigid, impermeable, flat plates that allows one to investigate mechanobiological responses of a monolayer of cells to changes in flow. Note the parabolic velocity profile, which is called a Poiseuille flow.

incompressible Newtonian response as well as a steady flow; that is, we can appropriately choose the culture media, the pump, and the geometry of the plates. Let us also assume that the effects of gravity on the flow field are negligible in comparison to the effects of the applied pressure gradient (i.e., difference between the upstream and downstream pressures), that the flow is unidirectional, and that the flow develops fully before reaching the cells. Hence, mathematically we have the following assumptions/restrictions:

1. Newtonian fluid ($\mu = \text{constant}$)
2. Incompressible flow ($\nabla \cdot \boldsymbol{v} = 0$)
3. Steady flow ($\partial \boldsymbol{v}/\partial t = \boldsymbol{0}$)
4. Unidirectional flow ($v_y = v_z = 0$)
5. Negligible body forces ($\boldsymbol{g} = \boldsymbol{0}$)
6. Fully developed flow ($\partial \boldsymbol{v}/\partial x = \boldsymbol{0}$)
7. 1-D flow ($\partial v_x/\partial z = 0$, $\partial v_x/\partial x = 0$)

We recommend at this point that the student use the worksheet from Sect. 8.7 to follow the subsequent derivations.

Note that assumption 6 suggests that there are no "end effects"; that is, the flow is the same along the length of the test section (recall from Chaps. 2 and 3 that we similarly avoided end effects in designing uniaxial experiments in biosolid mechanics for this simplified the analysis of the data). The constraint of an incompressible flow, in Cartesian coordinates, requires that mass balance according to [Eq. (8.14)]

$$\frac{\partial v_x}{\partial x} + \frac{\partial v_y}{\partial y} + \frac{\partial v_z}{\partial z} = 0, \tag{9.3}$$

which is clearly satisfied identically given our assumption that $\boldsymbol{v} = v_x(y)\hat{\boldsymbol{i}}$ only. Linear momentum balance, for a Newtonian behavior, requires that we satisfy the Navier–Stokes equation, which in Cartesian components is [Eqs. (8.36), (8.40), and (8.42)]

$$\begin{aligned}\hat{\boldsymbol{i}}: &-\frac{\partial p}{\partial x}+\mu\left(\frac{\partial^2 v_x}{\partial x^2}+\frac{\partial^2 v_x}{\partial y^2}+\frac{\partial^2 v_x}{\partial z^2}\right)+\rho g_x\\ &=\rho\left(\frac{\partial v_x}{\partial t}+v_x\frac{\partial v_x}{\partial x}+v_y\frac{\partial v_x}{\partial y}+v_z\frac{\partial v_x}{\partial z}\right),\end{aligned} \tag{9.4}$$

$$\begin{aligned}\hat{\boldsymbol{j}}: &-\frac{\partial p}{\partial y}+\mu\left(\frac{\partial^2 v_y}{\partial x^2}+\frac{\partial^2 v_y}{\partial y^2}+\frac{\partial^2 v_y}{\partial z^2}\right)+\rho g_y\\ &=\rho\left(\frac{\partial v_y}{\partial t}+v_x\frac{\partial v_y}{\partial x}+v_y\frac{\partial v_y}{\partial y}+v_z\frac{\partial v_y}{\partial z}\right),\end{aligned} \tag{9.5}$$

$$\begin{aligned}\hat{\boldsymbol{k}}: &-\frac{\partial p}{\partial z}+\mu\left(\frac{\partial^2 v_z}{\partial x^2}+\frac{\partial^2 v_z}{\partial y^2}+\frac{\partial^2 v_z}{\partial z^2}\right)+\rho g_z\\ &=\rho\left(\frac{\partial v_z}{\partial t}+v_x\frac{\partial v_z}{\partial x}+v_y\frac{\partial v_z}{\partial y}+v_z\frac{\partial v_z}{\partial z}\right).\end{aligned} \tag{9.6}$$

Canceling out terms consistent with the above assumptions (do it), we are left with

$$-\frac{\partial p}{\partial x}+\mu\frac{\partial^2 v_x}{\partial y^2}=0,\qquad -\frac{\partial p}{\partial y}=0,\qquad -\frac{\partial p}{\partial z}=0. \tag{9.7}$$

The second and third of these equations show that the pressure is a function of x at most (i.e., it is independent of y and z), thus the final governing differential equation is

$$\frac{dp}{dx}=\mu\frac{d^2 v_x}{dy^2}. \tag{9.8}$$

Note: The only way for a function of x (at most) to equal a function of y (at most) for all (x, y) is for each function to be a constant. Hence, the pressure gradient is constant and so too for the right-hand side of Eq. (9.8). Therefore, integrating this equation, we have

$$\mu\int\frac{d}{dy}\left(\frac{dv_x}{dy}\right)dy=\int\frac{dp}{dx}dy, \tag{9.9}$$

where, from Appendix 8 of Chap. 8, the integral of $d(something)/dy$ with respect to y yields that *something*, thus,

$$\mu \frac{dv_x}{dy} = \frac{dp}{dx} y + c_1. \tag{9.10}$$

Integrating again, we have

$$\mu \int \frac{d}{dy}(v_x) dy = \int \left(\frac{dp}{dx} y + c_1 \right) dy, \tag{9.11}$$

or

$$\mu v_x = \frac{dp}{dx} \frac{y^2}{2} + c_1 y + c_2. \tag{9.12}$$

As expected, we need two boundary conditions to find the two constants of integration because we began with a second-order differential equation. Enforcing the no-slip condition (that a fluid velocity equals that of a solid it contacts) at the bottom plate, $v_x(y=0)=0$, and likewise at the top plate, $v_x(y=h)=0$, allows us to find the constants

$$0 = \frac{dp}{dx} \frac{(0)^2}{2} + c_1(0) + c_2 \rightarrow c_2 = 0 \tag{9.13}$$

and

$$0 = \frac{dp}{dx} \frac{(h)^2}{2} + c_1(h) + 0 \rightarrow c_1 = -\frac{dp}{dx} \frac{h}{2}. \tag{9.14}$$

Thus, the velocity field $\boldsymbol{v} = v_x(y)\hat{\boldsymbol{i}}$ is described fully by the x-direction component,

$$v_x(y) = \frac{1}{2\mu} \frac{dp}{dx} \left(y^2 - hy \right). \tag{9.15}$$

Note that the velocity distribution is parabolic (Fig. 9.2); it is called a *Poiseuille flow* in honor of the French physician J. Poiseuille (1799–1869), who studied pressure–flow relations for blood flow. After checking that the boundary conditions are indeed satisfied, we could then calculate the maximum velocity of the flow. To do this, we must first determine that value of y at which the maximum occurs. This value can be calculated by taking the derivative of the velocity profile with respect to y and setting it equal to zero as follows:

$$\frac{dv_x}{dy} = \frac{1}{2\mu}\frac{dp}{dx}(2y - h) = 0 \rightarrow y = \frac{h}{2}. \tag{9.16}$$

Occurring at $y = h/2$, the maximum velocity is

$$v_x)_{\max} = -\frac{h^2}{8\mu}\frac{dp}{dx}. \tag{9.17}$$

Question: Does it make sense that this expression for the maximum velocity has a minus sign? The answer is yes, of course, because the pressure gradient must be negative to drive the flow in the positive x direction. In fact, returning to Eq. (9.8), which reveals that the pressure gradient equals a constant, say c_3, we have

$$\frac{dp}{dx} = c_3 \rightarrow \int \frac{dp}{dx}dx = \int c_3\, dx, \tag{9.18}$$

or

$$p = c_3 x + c_4. \tag{9.19}$$

The constants c_3 and c_4 can be found from upstream (proximal) and downstream (distal) pressures. For example, if $p = p_1$ at $x = x_1$ and $p = p_2$ at $x = x_2$, with $p_1 > p_2$ for $x_1 < x_2$ in order to drive the flow in the positive x direction, then

$$c_3 = \frac{p_1 - p_2}{x_1 - x_2}, \quad c_4 = -\left(\frac{p_1 x_2 - p_2 x_1}{x_1 - x_2}\right), \tag{9.20}$$

where c_3 is clearly negative and so too is the pressure gradient. Hence, the pressure field is

$$p = \left(\frac{p_1 - p_2}{x_1 - x_2}\right)x - \left(\frac{p_1 x_2 - p_2 x_1}{x_1 - x_2}\right). \tag{9.21}$$

To calculate the volumetric flow rate Q in the x direction, where $Q = \int_A (\boldsymbol{v} \cdot \boldsymbol{n})\, dA$, and $\boldsymbol{n} \equiv \hat{\boldsymbol{i}}$ in this problem, we have

$$Q = \int_A v_x dA = \int_0^h \int_0^w \frac{1}{2\mu}\frac{dp}{dx}\left(y^2 - hy\right)dzdy = \frac{w}{2\mu}\frac{dp}{dx}\int_0^h \left(y^2 - hy\right)dy, \tag{9.22}$$

or

$$Q = -\frac{h^3 w}{12\mu}\left(\frac{dp}{dx}\right), \tag{9.23}$$

where w is the width of the plates, which is assumed to be large compared to h so that edge effects are also negligible on each side. Again, the minus sign appears because the pressure gradient is negative and the value of Q is positive, as it should be. The average velocity (speed) of the flow is given by

$$\overline{v} = \frac{Q}{A} = -\frac{h^2}{12\mu}\frac{dp}{dx}. \tag{9.24}$$

We see, therefore, that $v_x)_{\max} = 3\overline{v}/2$.

Before finishing this problem by computing the fluid shear stress and associated wall shear stress, let us formalize two ideas that have been alluded to. First, we see from Eq. (9.15) that the computed velocity field $\boldsymbol{v}$ is a smooth function of position (x, y, z). Indeed, as we pick increasingly larger values of $y \in [0, h]$ the velocity changes in an ordered way, one in which the particles appear to travel in layers that slide relative to each other (Fig. 9.3). Such an ordered flow is called *laminar* for obvious reasons. In contrast, there are cases in which in fluid particles tend to have a random motion superimposed on an overall mean flow. Such a flow is termed *turbulent* (Fig. 9.3), which is mathematically very challenging to describe. Turbulence could occur in the flow between parallel plates if the velocity is very large or if the plates are very rough. This issue is not considered until Chap. 10, however. Second, we see from Eq. (9.15) that $\boldsymbol{v}$ does not depend on x; that is, the flow is assumed to be the same, within the region of interest, anywhere along the direction of flow. We would expect, of course, that the flow would not necessarily be the same at the point that it

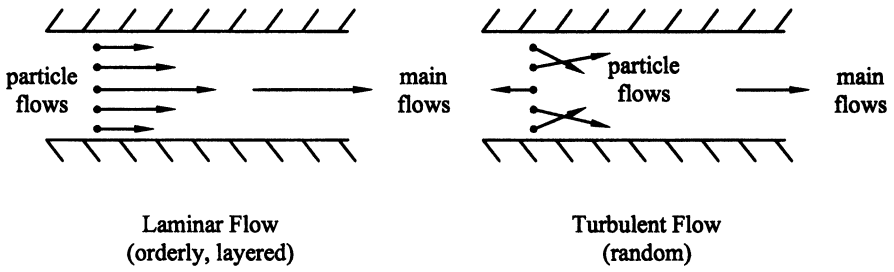

FIGURE 9.3 Schematic comparison of laminar versus turbulent flow. The former (*left*) is characterized by an orderly flow in which layers of fluid move relative to one another, whereas the latter (*right*) is characterized by a random flow superimposed on a net mean flow. A laminar flow can transition to a turbulent flow if the velocity increases sufficiently or if the surface of the constraining solid is sufficiently rough.

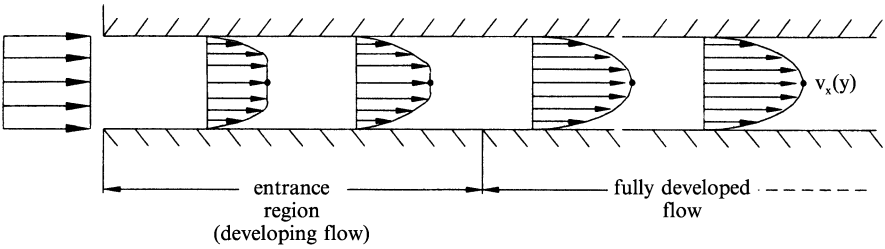

FIGURE 9.4 Because of the no-slip boundary condition for a viscous fluid, fluid particles slow (or stop) when they encounter a stationary solid. Because of the friction between layers of a viscous fluid, these slowed particles will, in turn, tend to slow neighboring fluid particles. Regions wherein such solid–fluid interactions are strong are called *boundary layers*. The boundary layer in a tube develops until the entire flow is affected. The entrance length is the region in which in the boundary layer is developing; thereafter the flow is called *fully developed*.

enters the parallel plates. Indeed, experiments reveal that the flow may develop from a uniform profile, to a blunted profile, to the final parabolic profile represented by Eq. (9.15). Illustrated in Fig. 9.4, such a region over which a flow develops is called an *entrance length*. Because the velocity field depends on multiple coordinates when developing, it is much more difficult to describe mathematically. For both computational and experimental convenience, such boundary value problems are often formulated so that the region of interest is within the *fully developed* region. In other cases, of course, the entrance length may play a key role in the flow and thus must be considered fully. This often requires numerical methods.

To calculate the shear stress on the cells, which is essential to enable the experimentalist to correlate changes in the production of various molecules by the endothelial cells with changes in flow, we need to calculate σ_{yz} at $y = 0$. Thus, recall the (Navier–Poisson) constitutive relation for Newtonian fluids [Eq. (7.66)], the yx equation of which is

$$\sigma_{yx} = 2\mu\left[\frac{1}{2}\left(\frac{\partial v_x}{\partial y} + \frac{\partial v_y}{\partial x}\right)\right]. \tag{9.25}$$

Given that $v_y \equiv 0$, we have from Eq. (9.15)

$$\sigma_{yx} = \mu\frac{\partial v_x}{\partial y} = \mu\left(\frac{1}{2\mu}\frac{dp}{dx}(2y - h)\right), \tag{9.26}$$

which we emphasize is the shear stress *in the fluid* at any point y (Fig. 9.5). By Newton's third law (for every action there is an equal and opposite reaction), *the wall shear stress* τ_w is equal and opposite the shear stress in the fluid at $y = 0$ and $y = h$. Note, therefore, that at $y = 0$,

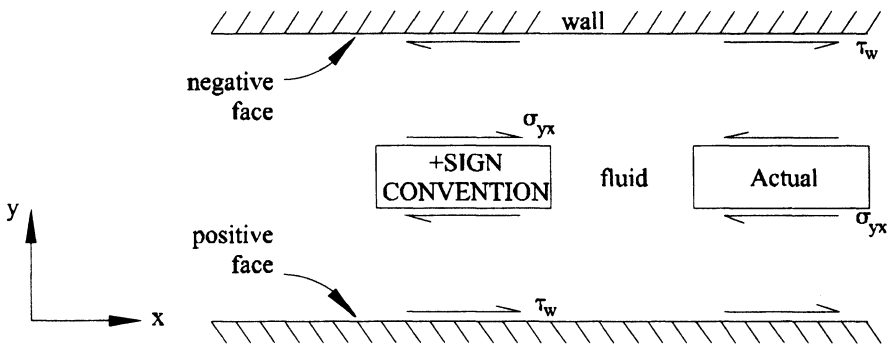

FIGURE 9.5 Positive sign convention for fluid stresses $\sigma_{(\text{face direction})}$ relative to a Cartesian coordinate system and the associated actual shear stresses in a fluid element σ_{xy} and on the wall τ_w in a parallel-plate experiment.

$$\sigma_{yx} = -\frac{h}{2}\left(\frac{dp}{dx}\right), \tag{9.27}$$

whereas at $y = h$,

$$\sigma_{yx} = \frac{h}{2}\left(\frac{dp}{dx}\right). \tag{9.28}$$

Because $dp/dx < 0$, σ_{yx} is positive at $y = 0$ and negative at $y = h$. Just as in statics (cf. Example A1.6 in Chap. 1), when the sign direction is taken positive but the value is found to be negative, we simply switch the direction of the force or stress. Hence, the shear stresses acting on a central fluid element act in the direction opposite the flow, whereas the fluid-induced wall shear stresses act in the positive x direction, as expected because the fluid tends to "push" on the solid, whereas the solid tends to "push back."

At this juncture, it is useful to note that endothelial cells not only produce various molecules in response to changes in the magnitude of the applied shear stress, they also tend to align themselves and elongate in the direction of the applied shear. Indeed, for this reason, the in vivo orientation and elongation of an endothelial cell provides indirect information on the value of the wall shear stress that exists at that point. Experimentally, then, it is useful to correlate changes in morphology and the production of vasoactive molecules with the magnitude of the applied shear stress, which in the parallel-plate device is now seen to be

$$\tau_w = \left|\frac{h}{2}\frac{dp}{dx}\right|, \tag{9.29}$$

or in terms of the volumetric flow rate Q, from Eq. (9.23),

$$\tau_w = \frac{6\mu Q}{wh^2}. \tag{9.30}$$

Not all parallel-plate experiments are designed the same, however. In some cases, investigators leave a small gap of air (actually 95 % air and 5 % CO_2) between the upper plate and the fluid, with the cells cultured on the bottom plate. In this case, it can be shown that (see Exercise 9.3)

$$\tau_w = \frac{3\mu Q}{wh^2}. \tag{9.31}$$

Clearly, therefore, theory is essential in the design and interpretation of experiments.

Observation 9.1. Many investigators have used parallel-plate devices to subject cultured endothelial or epithelial cells to well-controlled steady or pulsatile shear stresses and to monitor their responses. Here, however, let us consider but a few of the early findings on endothelial cells as recorded in Chap. 6 in Frangos (1993), studies which began in 1974 but began to attract heightened attention around 1981.

Endothelial cells are often taken from either the bovine aorta (BAEC) or the human umbilical vein (HUVEC). Regardless, the cells are typically cultured on glass slides coated with synthetic (e.g., polyester or Mylar) or biologic (elastin or fibronectin) substrates and exposed to a 37 °C culture media (often with 2–20 % fetal bovine serum and antibiotics) and a 95 % air/5 % CO_2 gas mixture. After reaching confluence on the substrate, the cells are typically subjected to laminar flows (often with the quantity $\rho\bar{v}h/\mu \leq 100$) for periods of hours to days. Flows between parallel plates tend to become turbulent only after $\rho\bar{v}h/\mu > 1,400$; it will be shown later that this nondimensional combination of terms is called the Reynolds' number, an important parameter in classifying many flows.

Among other results, it has been shown that endothelial cells tend to have a polygonal shape under static conditions, but in response to a constant shear stress ~ 1–10 Pa, the cells tend to elongate and then align with the direction of flow within 1–4 h of exposure to the shear (Fig. 9.6). Associated with these morphological changes are changes in the organization of the cytoskeleton. For example, the F-actin microfilaments tend to form dense peripheral bands under static conditions, bands that in the presence of shear stress tend to give way, over time, to the appearance of more centrally located stress fibers that are oriented in the direction of flow. Hence, the formation and orientation of the stress fibers coincide with gross changes in cell shape and orientation. That these two observations are coupled is revealed by tests in which cells are

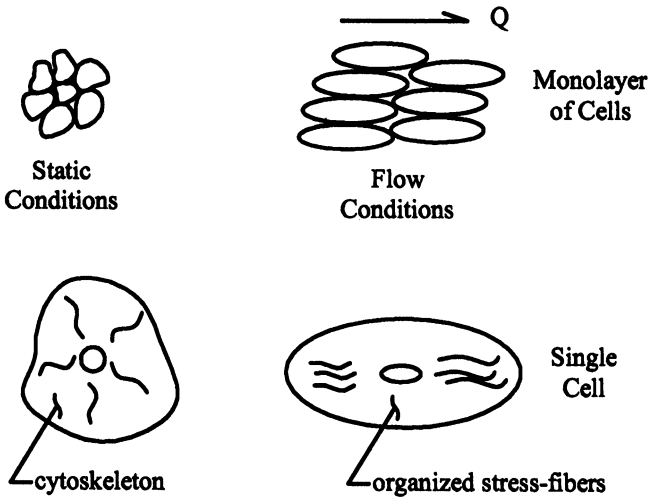

FIGURE 9.6 Schema of the effects of fluid flow on the shape and constitution of endothelial cells. Whereas the cells tend to be polygonal in shape under no-flow conditions, they tend to elongate and reorient with the direction of flow. Such shape changes are accompanied by changes in the cytoskeleton that include the production and orienting of stress fibers (cf. Fig. 1.5) in the direction of flow.

exposed to cytochalasin B, which disrupts actin assembly. Cells so treated do not elongate significantly in response to increases in shear stress. The intermediate filament vinculin, which participates in focal adhesion complexes, shows similar changes. Whereas vinculin may form nearly uniformly around the periphery of a cell under static conditions, it appears to localize at the upstream edge of cells subjected to flow. Hence, cells change their adhesion characteristics in response to flow. Indeed, studies have also shown that endothelial cells produce and organize fibronectin, an important extracellular adhesion molecule, which aids alignment in the direction of flow. Interestingly, this production tends to be diminished (with respect to static controls) early on during the exposure to flow, when the cell needs to be mobile and realign, but to be increased after alignment. Understanding cell–matrix interactions is obviously critical to understanding overall vascular biology.

In summary, parallel-plate experiments have revealed tremendous insights into correlations between shear stress and changes in cell morphology, cytoskeletal organization, the production of a host of molecules (vasoactive, growth regulatory, inflammatory, degradatory, and adhesive), and the production of extracellular matrix. The primary caveat, however, is that because cells are so sensitive to their environment, one must be cautious when trying to extrapolate

results in culture to in vivo settings. Cell response likely depends primarily on its recent history (including an initial growth under static conditions), the particular substrate and its possible deformation, the specific culture media (i.e., chemical milieu, including antibiotics and growth factors), the flow characteristics (steady, pulsatile, laminar, turbulent), and cell–cell and cell–matrix interactions. Much remains to be learned.

Example 9.1 It appears that Rosen et al. (1974) first showed in vitro that endothelial cells alter their production of a specific molecule (histamine) in response to altered shear stresses. They accomplished this using cultured cells placed within a parallel-plate device. Their device was $1.3 \times 1.3 \times 23.5$ cm in dimension, with the cells placed in the fully developed region (15 cm from the entrance). Because the flow chamber was not much wider than it was deep, however, the equations to compute the wall shear stress differed from Eq. (9.30). Ensuring that $h \ll w$ allows Eq. (9.30) to be used and facilitates the easy design and interpretation of the experiment. Toward this end, let us consider the work by Levesque and Nerem (1985). Their flow chamber was $0.025 \times 1.3 \times 5$ cm in dimension; hence, $h \ll w$ and our equations hold. They plotted the morphological measures for the cells versus wall shear stress τ_w, which they computed as

$$\tau_w = \frac{6\mu^2}{\rho h^2}\mathrm{Re},$$

where Re is the Reynolds' number. Show that this relation is correct.

Solution: As noted earlier, let the Reynolds' number be given by $\mathrm{Re} = \rho\bar{v}h/\mu$. Recall, therefore, that [from Eq. (9.24)]

$$\bar{v} = -\frac{h^2}{12\mu}\frac{dp}{dx} \rightarrow \frac{dp}{dx} = -\frac{12\mu\bar{v}}{h^2};$$

hence, from Eq. (9.29),

$$\tau_w = \left|\frac{h}{2}\frac{dp}{dx}\right| = \left|\frac{h}{2}\left(-\frac{12\mu\bar{v}}{h^2}\right)\right| = \left|-\frac{6\mu\bar{v}}{h}\right|.$$

Now, simply multiply by "one," namely

$$\tau_w = \left|-\frac{6\mu\bar{v}}{h}\left(\frac{h}{h}\frac{\rho}{\rho}\frac{\mu}{\mu}\right)\right| = \left|-\frac{6\mu^2}{h^2\rho}\left(\frac{\rho\bar{v}h}{\mu}\right)\right| = \frac{6\mu^2}{h^2\rho}\mathrm{Re},$$

with $\rho > 0$ and $\mathrm{Re} > 0$ by definition, thus yielding our desired result.

Note, too, that Levesque and Nerem stated that $\mathrm{Re} < 2{,}000$ ensured a laminar flow, and they subjected the cells to steady shear stresses of 1.0, 3.0, and 8.5 Pa for up to 24 h. Given that the viscosity and density where assumed to equal those of water and that $h = 250$ μm, find the exact values of Re for their reported values of τ_w to check if $\mathrm{Re} < 2{,}000$. Finally, note a few of their findings: "After 24 h of exposure at shear stresses of 30 and 85 dyn/cm^2, there was a significant reduction in cell surface area, an increase in cell perimeter and length, and a decrease in cell width ... the more elongated cells have a higher degree of alignment with the flow axis. This effect becomes accentuated with increasing shear stress." Note that 1 dyn/cm^2 = 0.1 Pa.

Example 9.2

The flow of water at room temperature ($\mu = 1.0 \times 10^{-3}$ N s/m^2) between parallel plates need not be due to a pressure gradient; one can also generate a flow by moving the plates relative to each other while maintaining the gap distance at a constant value. Thus, consider the flow in Fig. 9.7, where the top plate is moving at a constant velocity $U_0 = 0.1131$ m/s with no pressure gradient in the x direction. The fluid layer is 2 mm thick and the plate is 1 m wide. Use the Navier–Stokes equation for Newtonian flows to find (a) the velocity field, (b) the volumetric flow rate, and (c) the shear stress field.

Solution: Given

$$U_0 = 0.1131 \frac{\mathrm{m}}{\mathrm{s}}, \quad h = 2\,\mathrm{mm}, \quad w = 1\,\mathrm{m}, \quad \frac{dp}{dx} = 0 \ \frac{\mathrm{Pa}}{\mathrm{m}}.$$

Assume

1. Newtonian fluid ($\mu =$ constant)
2. Incompressible flow ($\nabla \cdot \boldsymbol{v} = 0$)

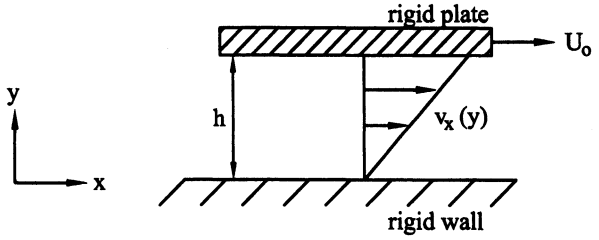

FIGURE 9.7 Couette flow induced by the relative motion of an *upper plate*, at constant velocity U_0, relative to a fixed rigid plate at the *bottom*. The associated velocity profile in the fluid is linear and, consequently, the fluid shear stress is uniform.

3. Steady flow ($\partial \boldsymbol{v}/\partial t = \boldsymbol{0}$)
4. Unidirectional flow ($v_y = v_z = 0$)
5. Negligible body forces ($\boldsymbol{g} = \boldsymbol{0}$)
6. Fully developed flow ($\partial \boldsymbol{v}/\partial x = \boldsymbol{0}$)
7. 1-D flow ($\partial v_x/\partial z = 0$, $\partial v_x/\partial x = 0$)
8. No pressure gradient in x ($\partial p/\partial x = 0$)

Mass balance is given by Eq. (9.3); it is again satisfied identically because $\boldsymbol{v} = v_x(\mathrm{y})\hat{\boldsymbol{i}}$ only. The balance of linear momentum in Cartesian coordinates is given by Eqs. (9.4)–(9.6). Eliminate the terms that disappear given the above assumptions and show that we have

$$\mu \frac{\partial^2 v_x}{\partial y^2} = 0, \qquad -\frac{\partial p}{\partial y} = 0, \qquad -\frac{\partial p}{\partial z} = 0.$$

The second and third equations, together with assumption 8, reveal that $p =$ constant. Hence, in the absence of a pressure-driven flow, the governing differential equation of motion is

$$\mu \frac{d^2 v_x}{dy^2} = 0.$$

Integrating twice with respect to y, we obtain

$$\mu v_x = c_1 y + c_2.$$

Invoking the no-slip condition at the bottom plate, $v_x(y = 0) = 0$, and the no-slip condition at the top plate, $v_x(y = h) = U_0$, we find that

$$0 = c_1(0) + c_2 \rightarrow c_2 = 0,$$

$$\mu U_0 = c_1(h) + 0 \rightarrow c_1 = \frac{\mu U_0}{h}.$$

Thus, the velocity profile is

$$v_x(y) = \frac{U_0}{h} y,$$

which is called a *Couette flow*. The volumetric flow rate Q, with $\boldsymbol{n} = \hat{\boldsymbol{i}}$, is thus given by

$$Q = \int_A v_x dA = \int_0^h \int_0^w \frac{U_0}{h} y \, dz \, dy \rightarrow Q = \frac{U_0 w h}{2}.$$

To calculate the shear stress, recall again that for Newtonian fluids,

$$\sigma_{yx} = 2\mu \left[\frac{1}{2} \left(\frac{\partial v_x}{\partial y} + \frac{\partial v_y}{\partial x} \right) \right],$$

where, consistent with the assumptions, $v_y \equiv 0$. Hence,

$$\sigma_{yx} = \mu \frac{\partial v_x}{\partial y} \rightarrow \sigma_{yx} = \mu \frac{U_0}{h},$$

or in terms of the volumetric flow rate Q,

$$\sigma_{yx} = \frac{2\mu Q}{w h^2}.$$

In contrast to the pressure-driven flow wherein σ_{yx} varied with position y and indeed went to zero at $y = h/2$, we see that σ_{yx} is constant in this Couette flow. Moreover, because the computed value of σ_{yx} is everywhere positive, each fluid element experiences a *simple shear* (cf. Fig. 7.7). The wall shear stress τ_w is equal and opposite the fluid shear stress at $y = 0$ and h.

As we emphasize throughout, although the problem statement requires a specific computation, it is always better to first solve the problem generally. Now that we have the general relations, we can substitute the numerical values given in the problem statement into our equations for the volumetric flow rate and the shear stress. They are respectively

$$Q = \frac{1}{2} \left(0.1131 \frac{\text{m}}{\text{s}} \right) (1\,\text{m})(0.002\,\text{m}) = 0.000113 \frac{\text{m}^3}{\text{s}} = 113 \frac{\text{mL}}{\text{s}},$$

$$|\tau_w| = \frac{\mu U_0}{h} = \frac{\left(1.0 \times 10^{-3} \text{N s/m}^2 \right) (0.1131 \ \text{m/s})}{0.002\,\text{m}} \approx 0.0566 \frac{\text{N}}{\text{m}^2} = 0.0566\,\text{Pa}.$$

We will discover in Sect. 9.3.3 that this simple (general) solution has important implications in various real-world problems, including determination of the viscosity of a fluid.

Example 9.3 Fluid flow down an inclined plane is influenced by the force of gravity. Consider the flow in Fig. 9.8, where a fluid film is subjected to the effects of gravity alone. Assume that the height of the fluid layer, h, remains constant and that there is no pressure gradient in the x direction. Use the Navier–Stokes equation for steady, incompressible Newtonian flows, given the coordinate system in the figure, to find (a) the pressure distribution in the y direction and (b) the velocity field.

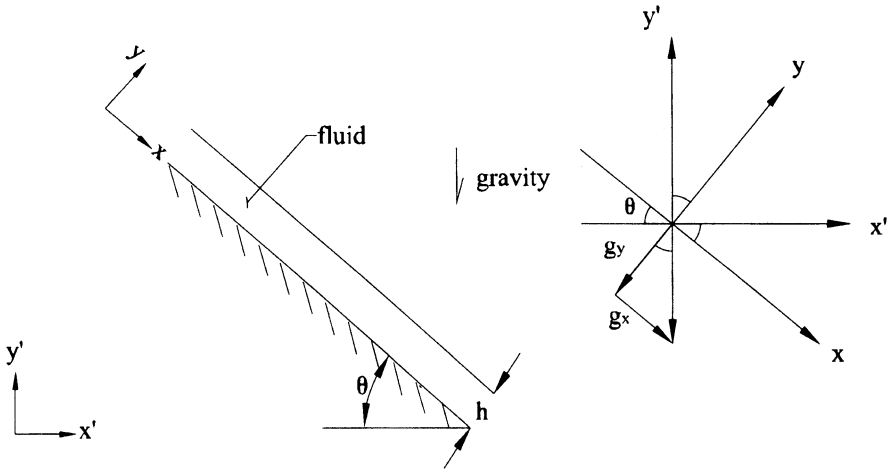

FIGURE 9.8 Uniform thickness flow of a Newtonian fluid down an inclined surface. The upper surface of the fluid is exposed to quiescent air at atmospheric pressure (i.e., zero pressure gauge), which is thus called a free surface. The only body force is gravity.

Solution:

Assume

1. Newtonian fluid ($\mu = \text{constant}$)
2. Incompressible flow ($\nabla \cdot \boldsymbol{v} = 0$)
3. Steady flow ($\partial \boldsymbol{v}/\partial t = \boldsymbol{0}$)
4. Unidirectional laminar flow ($v_y = v_z = 0$)
5. Fully developed flow ($\partial \boldsymbol{v}/\partial x = \boldsymbol{0}$)
6. 1-D flow ($\partial v_x/\partial z = 0$, $\partial v_x/\partial x = 0$)
7. No pressure gradient in x ($\partial p/\partial x = 0$)
8. Shear stress due to airflow over the surface of the film is negligible ($\sigma_{yx(\text{air})} \approx 0$)

The balance of mass, given by Eq. (9.3), is again satisfied identically because $\boldsymbol{v} = v_x(y)\hat{\boldsymbol{i}}$ only. The balance of linear momentum, in Cartesian coordinates, is

given by Eqs. (9.4)–(9.6). Given the above assumptions, we again eliminate the appropriate terms and find that we are left with

$$\mu\frac{\partial^2 v_x}{\partial y^2}+\rho g_x=0,\qquad -\frac{\partial p}{\partial y}+\rho g_y=0,\qquad -\frac{\partial p}{\partial z}=0,$$

wherein, due to gravity $\boldsymbol{g}=-g\hat{\boldsymbol{j}}'$, we include the body force acting on the fluid. This force can be resolved into x and y components using the given coordinate systems (remember that coordinate systems should be picked for convenience). Doing so, we see that $g_x=g\sin\theta$ and $g_y=-g\cos\theta$ Thus, we have

$$\mu\frac{\partial^2 v_x}{\partial y^2}+\rho g\sin\theta=0,\qquad -\frac{\partial p}{\partial y}-\rho g\cos\theta=0,\qquad -\frac{\partial p}{\partial z}=0.$$

Clearly, the pressure is a function of y alone, which can be determined via

$$\frac{dp}{dy}=-\rho g\cos\theta,$$

which, upon integration, yields

$$p(y)=-\rho g(\cos\theta)y+c.$$

Now, we need a boundary condition to solve for the constant c. Knowing that the surface of the fluid film, at $y=h$, is subjected to atmospheric pressure conditions or P_{atm}, we get

$$P_{\text{atm}}=-\rho g(\cos\theta)h+c\rightarrow c=P_{\text{atm}}+\rho g(\cos\theta)h.$$

Thus, the (absolute) pressure distribution in the y direction is

$$p(y)=\rho g(h-y)\cos\theta+P_{\text{atm}}.$$

The gauge pressure is the absolute pressure minus atmospheric pressure. We also see from the x-direction equation of motion that the velocity is a function of y alone, thus the final governing differential equation of motion is

$$\frac{d^2 v_x}{dy^2}=-\frac{\rho g\sin\theta}{\mu}.$$

Integrating twice, we obtain

$$v_x(y) = -\frac{\rho g \sin\theta}{2\mu} y^2 + c_1 y + c_2.$$

Invoking the no-slip condition at the face of the inclined plane, $v_x(y=0)=0$, we find that

$$0 = 0 + c_1(0) + c_2 \rightarrow c_2 = 0.$$

Now, we need an appropriate boundary condition for the top surface of the fluid film. Recall that when we formulated the problem, we assumed that the shear stress due to airflow over the fluid film was negligible. Hence,

$$\sigma_{yx(\text{air})} \approx 0 \rightarrow \sigma_{yx(\text{fluid})}\Big|_{y=h} = \mu \frac{\partial v_x}{\partial y}\bigg|_{y=h} = 0,$$

where $\sigma_{yx(\text{air})}\big|_{y=h} = -\sigma_{yx(\text{fluid})}\big|_{y=h}$. Thus,

$$\mu \frac{\partial v_x}{\partial y}\bigg|_{y=h} = 0 = \mu\left(-\frac{\rho g h \sin\theta}{\mu} + c_1\right),$$

or

$$c_1 = \frac{\rho g h \sin\theta}{\mu}.$$

Thus, the velocity profile is

$$v_x(y) = \frac{\rho g \sin\theta}{\mu}\left(yh - \frac{y^2}{2}\right).$$

Once we are finished (i.e., when we have found the velocity and pressure fields), we should always examine special cases, the correctness of which gives us added confidence in our formulation and solution. Note, therefore, that $v_x = 0$ when $\theta = 0$, as expected, because there is no pressure gradient or moving solid to drive the flow. In conclusion, then, having computed the velocity and pressure fields, we can now calculate any quantity of interest, such as the shear stress, acceleration, or vorticity. This is left as an exercise, however.

9.2 Steady Flow in Circular Tubes

9.2.1 Biological Motivation

Most conduits for the flow of fluids within the body are cylindrical or nearly so, such as arteries, veins, airways, and ureters. Again, because of the sensitivity of endothelial and epithelial cells to applied shear stresses, it is important to have full solutions for these flows. In this way, we can understand better both physiology and pathology, and perhaps, most importantly, we can design better strategies for diagnosis and treatment. As it is well known, atherosclerosis is one of the leading causes of morbidity and mortality in the Western world. Briefly, atherosclerosis is a disease of the innermost layer of the arterial wall, the intima; it generally begins as a localized accumulation of lipids, sometimes called "fatty streaks," that form in preferential sites within the vascular tree. Over time, these lesions become more complex due to the accumulation of proliferating smooth muscle cells, excess matrix proteins (e.g., collagen) synthesized by the smooth muscle, and, in later stages, calcium and necrotic debris (Fig. 9.9). As a result, these lesions begin to compromise the lumen, the region of the obstruction being called a *stenosis*.

The three primary methods of treating atherosclerosis all rely heavily on biomechanics, or at least they should. Surgery typically involves the implantation of a graft that either replaces or bypasses the diseased region; angioplasty involves the dilatation of a balloon-tipped catheter within the stenosis to expand the lumen; and stenting involves the deployment of a metallic device to "hold open" the diseased region (see Fig. 9.10a–c). Currently, vascular grafts consist of two basic classes: *Synthetic grafts* are fabricated from man-made materials such as Dacron (see Fig. 10.5), whereas *natural grafts* include the use of arteries (e.g., internal mammary) or veins (saphenous) from other vascular beds within the patient. Finally, note that an exciting frontier is that of *tissue engineering* wherein one seeks to grow replacement tissues from the patient's cells. Herein, let us consider briefly the case of vein grafts.

Perhaps the first research into the potential use of veins as arterial grafts was that of Carrel and Guthrie (1906). Briefly, they transplanted canine jugular veins into the position of the carotid artery. Whereas the carotid artery typically experiences pulsatile flows with luminal pressures changing from ~80 to 120 mm Hg, the jugular vein typically experiences nearly steady flows and a luminal pressure ~5 mm Hg. Because *structure closely follows function in the body*, the normal microstructure and gross morphology of the jugular vein is (as expected) much different from that of the carotid artery. In humans in particular, the typical luminal diameter is ~10.1 mm in the jugular vein and ~6.4 mm in the nearby carotid artery (Mortensen et al. 1990).

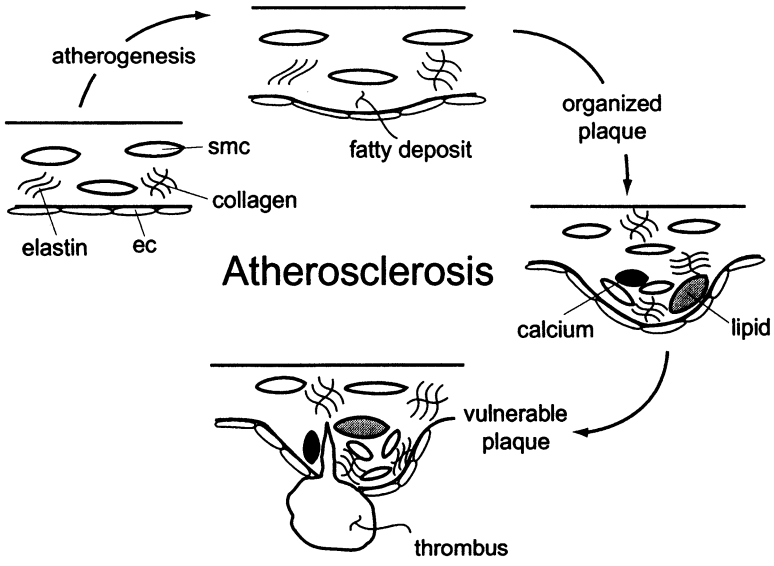

FIGURE 9.9 Schema of the atherosclerotic process, potentially leading from a fatty streak (defined by the accumulation of lipids in the subintimal space), to an organized plaque consisting of excess cells and matrix as well as lipids and calcium, to a possibly vulnerable plaque that may rupture and thrombose. Vulnerable plaques appear to be characterized by a thin collagenous cap that covers a softer core containing significant amounts of necrotic debris and lipids. Understanding the rupture of plaque thus requires knowledge of the solid mechanics (properties of and stresses in the plaque) and the fluid mechanics (the fluid-induced loads on the plaque, which serve as boundary conditions in the solid mechanics problem). *ec* endothelial cell, *smc* smooth muscle cell. (From Humphrey (2002), with permission).

As expected, Carrel and Guthrie found that veins transplanted to the arterial system thicken dramatically in response to increased pressure (Fig. 9.11). In order to understand, and ultimately to control, the response of vein grafts to their new environment (i.e., their growth and remodeling processes), we must understand well the normal properties and environment of the vein itself. Indeed, as we just saw in Sect. 9.1, the activity of the endothelium is tightly controlled by the wall shear stress τ_w, and as we saw in Chap. 6, the activity of the intramural cells (smooth muscle and fibroblasts) is tightly controlled by the pressure-induced circumferential stress. Here, let us begin such a study by considering a simple case—the steady, incompressible flow of a Newtonian fluid in a nondistending circular tube—in order to determine the wall shear stress in terms of clinically measurable quantities. In this case, the Navier–Stokes equations admit another exact solution. Thus, consider the tube in Fig. 9.12, of inner radius a, wherein the flow is one dimensional (e.g., no lateral diffusion or secondary flows).

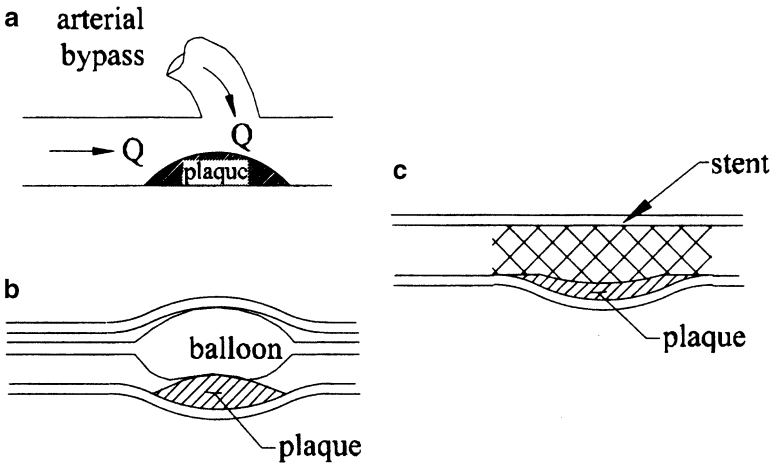

FIGURE 9.10 Three methods by which obstructive atherosclerotic lesions are treated: bypass grafts seek to restore flow to distal tissue by bypassing the obstruction, balloon angioplasty seeks to modify the plaque and weaken the wall so that it can distend more under normal physiologic pressures, and intravascular stents seek to hold open the lumen. Some stents are made of shape-memory alloys, and thus require advanced theories of material behavior.

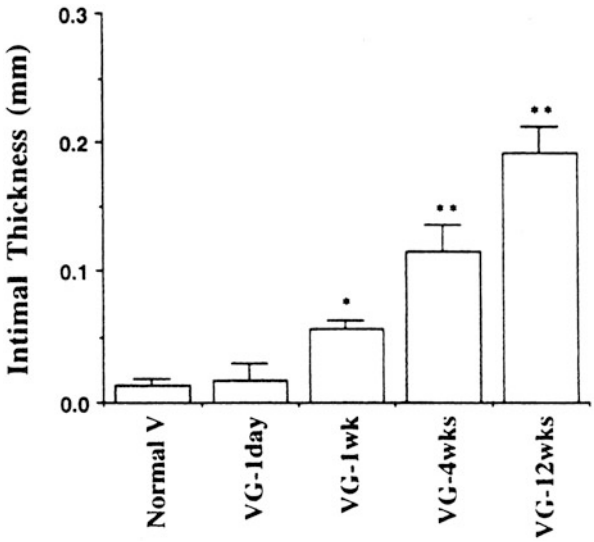

FIGURE 9.11 Intimal thickening over time of a vein used as a graft in the arterial system; note that the asterisks denote statistical significance; *VG* Vein graft. (From Han et al. (1998), with permission from ASME.).

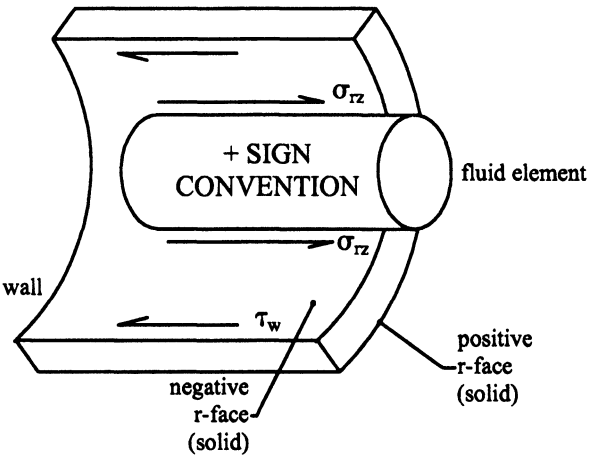

FIGURE 9.12 Sign convention for fluid shear stresses σ_{rz} for flow in a rigid circular tube.

9.2.2 Mathematical Formulation

Because of the circular geometry, it will prove convenient to employ cylindrical coordinates. Let us assume further the following:

1. Newtonian fluid ($\mu = \text{constant}$)
2. Incompressible flow ($\nabla \cdot \boldsymbol{v} = 0$)
3. Steady flow ($\partial \boldsymbol{v}/\mathrm{d}\partial t = \mathbf{0}$)
4. Axial flow only ($v_r = v_\theta = 0$)
5. Fully developed flow ($\partial \boldsymbol{v}/\partial z = \mathbf{0}$)
6. Axisymmetric flow ($\partial \boldsymbol{v}/\partial \theta = \mathbf{0}$)
7. Negligible body forces ($\boldsymbol{g} = \mathbf{0}$)
8. Laminar flow

Note that the flow tends to be fully developed when its distance from the entrance of the tube is greater than

$$L_e \sim 0.06\left(\frac{\rho \bar{v} D}{\mu}\right) D, \tag{9.32}$$

where $\bar{v}$ is the mean forward velocity and D is the diameter. This length L_e is called the *entrance length*. Moreover, the flow tends to remain laminar if

$$\mathrm{Re} \equiv \frac{\rho \bar{v} D}{\mu} < 2{,}100 \tag{9.33}$$

where this combination of terms is the aforementioned Reynolds' number.

Mass balance in cylindrical coordinates [Eq. (8.15)] requires that

$$\frac{1}{r}\frac{\partial(rv_r)}{\partial r}+\frac{1}{r}\frac{\partial v_\theta}{\partial\theta}+\frac{\partial v_z}{\partial z}=0, \tag{9.34}$$

which again is satisfied identically given this set of assumptions (i.e., v_z is a function of r alone). In cylindrical coordinates, linear momentum balance (i.e., the Navier–Stokes equation, $-\nabla p+\mu\nabla^2\boldsymbol{v}+\rho\boldsymbol{g}=\rho\boldsymbol{a}$) requires [Eqs. (8.46), (8.47), and (8.48)] the following:

$$\begin{aligned}\hat{\boldsymbol{e}}_r:\quad &-\frac{\partial p}{\partial r}+\mu\left[\frac{\partial}{\partial r}\left(\frac{1}{r}\frac{\partial(rv_r)}{\partial r}\right)+\frac{1}{r^2}\frac{\partial^2 v_r}{\partial\theta^2}-\frac{2}{r^2}\frac{\partial v_\theta}{\partial\theta}+\frac{\partial^2 v_r}{\partial z^2}\right]+\rho g_r\\ &=\rho\left(\frac{\partial v_r}{\partial t}+v_r\frac{\partial v_r}{\partial r}+\frac{v_\theta}{r}\frac{\partial v_r}{\partial\theta}-\frac{v_\theta^2}{r}+v_z\frac{\partial v_r}{\partial z}\right),\end{aligned} \tag{9.35}$$

$$\begin{aligned}\hat{\boldsymbol{e}}_\theta:\quad &-\frac{1}{r}\frac{\partial p}{\partial\theta}+\mu\left[\frac{\partial}{\partial r}\left(\frac{1}{r}\frac{\partial(rv_\theta)}{\partial r}\right)+\frac{1}{r^2}\frac{\partial^2 v_\theta}{\partial\theta^2}+\frac{2}{r^2}\frac{\partial v_r}{\partial\theta}+\frac{\partial^2 v_\theta}{\partial z^2}\right]+\rho g_\theta\\ &=\rho\left(\frac{\partial v_\theta}{\partial t}+v_r\frac{\partial v_\theta}{\partial r}+\frac{v_\theta}{r}\frac{\partial v_\theta}{\partial\theta}+\frac{v_r v_\theta}{r}+v_z\frac{\partial v_\theta}{\partial z}\right),\end{aligned} \tag{9.36}$$

$$\begin{aligned}\hat{\boldsymbol{e}}_z:\quad &-\frac{\partial p}{\partial z}+\mu\left[\frac{1}{r}\frac{\partial}{\partial r}\left(r\frac{\partial v_z}{\partial r}\right)+\frac{1}{r^2}\frac{\partial^2 v_z}{\partial\theta^2}+\frac{\partial^2 v_z}{\partial z^2}\right]+\rho g_z\\ &=\rho\left(\frac{\partial v_z}{\partial t}+v_r\frac{\partial v_z}{\partial r}+\frac{v_\theta}{r}\frac{\partial v_z}{\partial\theta}+v_z\frac{\partial v_z}{\partial z}\right).\end{aligned} \tag{9.37}$$

After eliminating terms consistent with the above assumptions (do it using the worksheet in Sect. 8.7), we are left with

$$-\frac{\partial p}{\partial r}=0,\qquad -\frac{\partial p}{\partial\theta}=0,\qquad -\frac{\partial p}{\partial z}+\mu\left[\frac{1}{r}\frac{\partial}{\partial r}\left(r\frac{\partial v_z}{\partial r}\right)\right]=0. \tag{9.38}$$

The first two equations show that the pressure is a function of z at most. Noting that the velocity is a function of r alone, the only way that a function of z (the pressure gradient) can equal a function of r (the viscous term) for all (r, z) is for both functions to be a constant. Thus, the pressure gradient is a constant, and so too for the viscous term; hence,

$$\frac{dp}{dz} = \mu\left[\frac{1}{r}\frac{\partial}{\partial r}\left(r\frac{\partial v_z}{\partial r}\right)\right] \tag{9.39}$$

is the governing differential equation. Multiplying through by r and integrating this equation with respect to r, we obtain

$$\int \frac{\partial}{\partial r}\left(r\frac{\partial v_z}{\partial r}\right)dr = \int \frac{1}{\mu}\frac{dp}{dz}r\,dr, \tag{9.40}$$

or

$$r\frac{\partial v_z}{\partial r} = \frac{1}{2\mu}\frac{dp}{dz}r^2 + c_1. \tag{9.41}$$

Dividing through by r and integrating again, we have or

$$\int \frac{\partial}{\partial r}(v_z)dr = \int \left(\frac{1}{2\mu}\frac{dp}{dz}r + \frac{c_1}{r}\right)dr, \tag{9.42}$$

or

$$v_z(r) = \frac{1}{4\mu}\frac{dp}{dz}r^2 + c_1 \ln r + c_2. \tag{9.43}$$

In order for $v_z(r)$ to be finite at all r, including the centerline at $r = 0$, c_1 must be zero (because the natural logarithm is not finite at $r = 0$). Note that this condition is not a boundary condition; rather, it is an extra condition that requires that the solution be physically reasonable. Similar "additional conditions" were used in earlier chapters on biosolid mechanics, as, for example, the requirement that the deflection be the same in a bone and prosthesis or in the left and right halves of a transversely loaded beam. The identification of such conditions comes primarily from intuition or experience. Next, applying the no-slip boundary condition at the wall of the cylinder, $v_z(r = a) = 0$, we find that

$$0 = \frac{1}{4\mu}\frac{dp}{dz}a^2 + c_2 \rightarrow c_2 = -\frac{1}{4\mu}\frac{dp}{dz}a^2. \tag{9.44}$$

Thus, the (fully developed) velocity field is $\boldsymbol{v} = v_z(r)\hat{\boldsymbol{e}}_z$, where

$$v_z(r) = \frac{1}{4\mu}\frac{dp}{dz}\left(r^2 - a^2\right) = \frac{-a^2}{4\mu}\frac{dp}{dz}\left(1 - \frac{r^2}{a^2}\right). \tag{9.45}$$

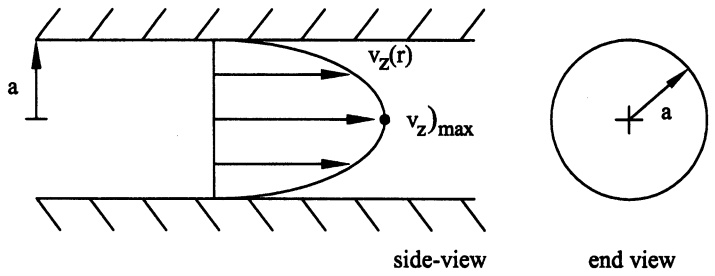

FIGURE 9.13 Velocity profile for the steady, laminar, fully developed, incompressible flow of a Newtonian fluid in a rigid circular tube. Like the flow between parallel plates, this parabolic profile is also called a Poiseuille flow.

Now, to calculate the maximum velocity in the flow field (Fig. 9.13), we must first determine the value of r at which the maximum occurs. This value can be calculated by taking the derivative of the velocity profile with respect to r and setting it equal to zero as follows:

$$\frac{dv_z}{dr} = \frac{1}{2\mu}\frac{dp}{dz}r = 0 \rightarrow r = 0. \tag{9.46}$$

The maximum velocity, at $r = 0$, is thus

$$v_z)_{\max} = v_z(r = 0) = -\frac{a^2}{4\mu}\left(\frac{dp}{dz}\right), \tag{9.47}$$

again realizing that the pressure gradient is negative in order to drive the fluid in the positive z direction; thus, the value of the maximum velocity is positive as it should be. To calculate the volumetric flow rate Q, we have (with $\boldsymbol{n} = \hat{\boldsymbol{e}}_z$ and $\boldsymbol{v} = v_z\hat{\boldsymbol{e}}_z$)

$$Q = \int_A v_z dA = \int_0^{2\pi}\int_0^a \left[\frac{1}{4\mu}\frac{dp}{dz}\left(r^2 - a^2\right)r\right]drd\theta, \tag{9.48}$$

where $dA = rd\theta dr$ or

$$Q = \frac{2\pi}{4\mu}\frac{dp}{dz}\left(\frac{r^4}{4} - \frac{a^2r^2}{2}\right)\Bigg|_0^a = -\frac{\pi a^4}{8\mu}\frac{dp}{dz}. \tag{9.49}$$

The average velocity (speed) of the flow is given by

$$\overline{v} = \frac{Q}{A} = \left(-\frac{\pi a^4}{8\mu}\frac{dp}{dz}\right)\left(\frac{1}{\pi a^2}\right) = -\frac{a^2}{8\mu}\frac{dp}{dz}. \tag{9.50}$$

To calculate the shear stress on the vessel wall τ_w, we need to calculate the shear stress in the fluid σ_{rz} at all r and then at $r = a$. Recall that for Newtonian fluids [Eqs. (7.64) and (7.58) of Chap. 7],

$$\sigma_{rz} = 2\mu\left[\frac{1}{2}\left(\frac{\partial v_z}{\partial r} + \frac{\partial v_r}{\partial z}\right)\right], \tag{9.51}$$

but given that $v_r \equiv 0$, we have

$$\sigma_{rz} = \mu\frac{\partial v_z}{\partial r} = \frac{dp}{dz}\frac{r}{2}, \tag{9.52}$$

again noting that dp/dz is negative. Hence, the direction of σ_{rz} is opposite its positive sign convention (Fig. 9.12) and the wall shear stress is

$$\tau_w = \left|\frac{dp}{dz}\frac{a}{2}\right| \tag{9.53}$$

in the positive z direction. From Eqs. (9.49) and (9.50), however, the pressure gradient is

$$\frac{dp}{dz} = -\frac{8\mu Q}{\pi a^4} \quad \text{or} \quad \frac{dp}{dz} = -\frac{8\mu\overline{v}}{a^2}; \tag{9.54}$$

hence the wall shear stress can be written as

$$\tau_w = \frac{4\mu Q}{\pi a^3} \quad \text{or} \quad \tau_w = \frac{4\mu\overline{v}}{a}. \tag{9.55}$$

The former result is one of the most often cited equations in vascular biology related to endothelial mechanotransduction [cf. Eq. (9.30)]. Nonetheless, we must remember all of the assumptions embodied in its derivation, including the assumptions of a rigid wall and steady flow.

Example 9.4 The so-called *skin friction coefficient* c_f is defined as the wall shear stress divided by the mean dynamic pressure. Find a formula for c_f for a steady flow in a rigid tube.

Solution: The *dynamic pressure* is defined as $\rho\overline{v}^2/2$, where $\overline{v}$ is a scalar measure of the mean velocity [i.e., the speed; see Bernoulli's equation (8.80)]. For the case of a tube flow, therefore, the mean dynamic pressure is

$$P_{dyn} = \frac{1}{2}\rho\bar{v}^2 = \frac{1}{2}\rho\left(-\frac{a^2}{8\mu}\frac{dp}{dz}\right)^2,$$

where the mean velocity is given by Eq. (9.50). Hence, in this case (Fung 1993),

$$c_f = -\frac{a}{2}\left(\frac{dp}{dz}\right)\left\{\frac{\rho}{2}\left[\frac{a^4}{64\mu^2}\left(\frac{dp}{dz}\right)^2\right]\right\}^{-1} = -64\mu^2\left[\rho a^3\left(\frac{dp}{dz}\right)\right]^{-1},$$

which, via Eq. (9.54), can be written as

$$c_f = \frac{-64\mu^2}{\rho a^3(-8\mu\bar{v}/a^2)} = \frac{16}{\rho(2a)\bar{v}/\mu} = \frac{16}{\mathrm{Re}},$$

where the Reynolds' number is

$$\mathrm{Re} = \frac{\rho\bar{v}d}{\mu},$$

with $d = 2a$ the diameter of the tube. Re is a very important nondimensional parameter in fluid mechanics; it will be discussed in greater depth in Chap. 10. In summary, the wall shear stress in this tube flow can also be written as

$$\tau_w = \frac{1}{2}\rho\bar{v}^2 c_f = \frac{1}{2}\rho\bar{v}^2\left(\frac{16}{\mathrm{Re}}\right).$$

For example, in the human aorta,

$$\bar{v} = 0.15\ \mathrm{m/s}, \qquad d = 0.03\ \mathrm{m}$$
$$\rho = 1{,}060\ \mathrm{kg/m^3}, \qquad \mu = 3.3 \times 10^{-3}\ \mathrm{N\,s/m^2};$$

hence,

$$\mathrm{Re} = \frac{(1{,}060\,\mathrm{kg/m^3})(0.15\mathrm{m/s})(0.03\,\mathrm{m})}{3.3 \times 10^{-3}\mathrm{N\,s/m^2}} = 1{,}445,$$

where 1 kg m/s^2 = 1 N. This value is less than that expected for turbulent flow (Re > 2,100); hence, our laminar assumption applies. Note, too, that the associated value of $\tau_w = 0.13$ kg/m s^2 = 0.13 Pa, which is within the reported range albeit lower than that which is usually reported (1.5 Pa).

9.3 Circumferential Flow Between Concentric Cylinders

Let us next consider a general case that has two important applications (Fig. 9.14): The steady, incompressible flow of a Newtonian fluid between two rigid, impermeable, circular cylinders, each of which can rotate at a different angular velocity. For example, such a problem describes the concentric cylinder viscometer wherein one seeks to measure the viscosity of a fluid by measuring the twisting moment (torque) T that is required to rotate the inner cylinder at angular velocity ω while the outer cylinder is fixed. Another application of this problem is the NASA bioreactor (Wolf and Schwarz, 1991).

9.3.1 Bioreactor Application

Atmospheric pressure near sea level is ~14.7 psi. If we estimate the surface area of our skin via a cylinder ~60 in. high and 12 in. in diameter, then the surface area is $\sim 2\pi(6)(60) = 2{,}260$ in^2. At 14.7 psi, therefore, our bodies resist an amazing ~33,250 lbs of total force. That we do not feel the "burden" of this load is an example of adaptation; that is, it is as if our skin senses gauge pressures, not absolute pressures, where $P_{\text{abs}} = P_{\text{atm}} + P_{\text{gauge}}$.

Likewise, our bodies are well accommodated to the normal gravitational pull of 1 g. It should not be surprising, therefore, that when astronauts experience microgravity in space, the cells in their bodies sense and seek to respond to this change. Because we plan to extend a human's duration in space via a voyage to Mars or other extended journey, we must understand better the responses of cells to a microgravity environment. Indeed, recall from Chap. 1 that the *Apollo* program in the 1960s provided an important motivation for the development of biomechanics.

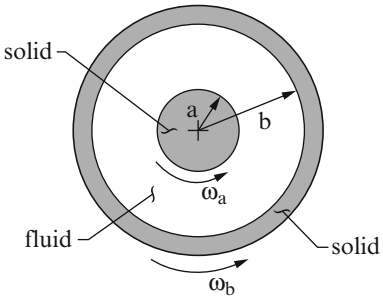

FIGURE 9.14 Steady flow of an incompressible Newtonian fluid between two concentric, rigid, circular cylinders which may rotate at different angular velocities ω_a and ω_b. In practice, the gap distance $h = b - a$ would be small in comparison to a; thus, the gap is exaggerated for illustrative purposes only.

Space-based experimentation is clearly the most natural approach to study the effects of microgravity, but it is also the most expensive. NASA scientists and engineers have thus sought Earth-based experiments to simulate the effects of microgravity; such tests should be both cost-effective and revealing. One such experiment is the so-called hindlimb unloading of a rat. Note, therefore, that any human activity on Earth that involves an upright posture (e.g., standing, walking, running) induces a normal gradient on the hydrostatic blood pressure from head to foot (cf. Example 8.3 of Chap. 8). Consequently, blood vessels in the legs may constrict to prevent blood from pooling in the lower extremities. In a microgravity environment, however, there is a loss of this normal head-to-foot gradient in pressure and there is an associated shift in fluids from the lower to the upper portions of the body. Such changes, if sustained over long periods, trigger adaptations in the cardiovascular system that can cause problems when the astronaut returns to Earth. For example, astronauts may become dizzy or faint when standing upright soon after their return to Earth. One way to examine the effects of such *orthostatic intolerance* is to induce similar head-to-foot fluid shifts in laboratory animals and then to study changes in vascular structure and function. In the hindlimb unloading experiment, a rat is suspended by its tail so that the hindlimbs are elevated and not weight bearing. As noted by Delp et al. (2000), this animal model "induces the cephalic fluid shift and postural muscle unloading that occur in microgravity. Additionally, the hindlimb unloaded animals manifest many of the adaptations that are characteristic of exposure to microgravity, including postural muscle atrophy, hypovolemia, a diminished capacity to elevate vascular resistance, orthostatic hypotension, and a reduced aerobic capacity." Of course, to understand fully such experiments, one must understand the associated biosolid and biofluid mechanics.

Another experimental setup to study the effects of microgravity is the so-called NASA *bioreactor*. Briefly, living cells are either allowed to float freely within a culture media contained between two concentric rotating cylinders or the cells are cultured on the walls of one of the cylinders. The basic idea is to confuse the cells as to which "direction is up," which is to say, to subject them to a changing gravitational vector and thereby simulate microgravity via the absence of a consistent gravitational field. More on these specific applications later. Here, let us formulate and solve the general problem (Fig. 9.14) independent of the specific application.

9.3.2 Mathematical Formulation

Let the fluid flow be in the θ and possibly r directions, with no-slip boundary conditions at $r = a$ and $r = b$ requiring v_θ to vary with radius. Hence, let $\boldsymbol{v} = v_r(r)\hat{\boldsymbol{e}}_r + v_\theta(r)\hat{\boldsymbol{e}}_\theta$ consistent with the following assumptions:

1. Newtonian fluid ($\mu = \text{constant}$)
2. Incompressible flow ($\nabla \cdot \boldsymbol{v} = 0$)

3. Steady flow ($\partial \boldsymbol{v}/\partial t = \boldsymbol{0}$)
4. $v_z = 0$
5. No change in the z direction ($\partial \boldsymbol{v}/\partial z = \boldsymbol{0}$)
6. Axisymmetric flow ($\partial \boldsymbol{v}/\partial \theta = \boldsymbol{0}$)
7. Negligible body forces ($\boldsymbol{g} = \boldsymbol{0}$)
8. Laminar flow

Recall that mass balance, in cylindrical coordinates, requires [Eq. (8.15)]

$$\frac{1}{r}\frac{\partial (rv_r)}{\partial r} + \frac{1}{r}\frac{\partial v_\theta}{\partial \theta} + \frac{\partial v_z}{\partial z} = 0, \tag{9.56}$$

which, upon invoking the above assumptions, reduces to

$$\frac{1}{r}\frac{\partial (rv_r)}{\partial r} = 0. \tag{9.57}$$

Multiplying through by r and integrating, we obtain

$$\int \frac{\partial (rv_r)}{\partial r} dr = \int 0\, dr \rightarrow rv_r = c_1 \quad \text{or} \quad v_r = \frac{c_1}{r}. \tag{9.58}$$

Applying the no-slip condition at the inner ($r = a$) or outer ($r = b$) walls of the cylinders, $v_r(r = a) = 0 = v_r(r = b)$, we get $c_1 = 0$. Thus, the velocity is zero in the r direction (in this idealized case), and we again have a unidirectional 1-D flow: $\boldsymbol{v} = v_\theta(r)\hat{\boldsymbol{e}}_\theta$ only. Recall, too, that the Navier–Stokes equation, $-\nabla p + \mu \nabla^2 \boldsymbol{v} + \rho \boldsymbol{g} = \rho \boldsymbol{a}$), in cylindrical coordinates is [Eqs. (8.46)–(8.48)]

$$\begin{aligned} \hat{\boldsymbol{e}}_r: \quad & -\frac{\partial p}{\partial r} + \mu \left[\frac{\partial}{\partial r}\left(\frac{1}{r}\frac{\partial (rv_r)}{\partial r} \right) + \frac{1}{r^2}\frac{\partial^2 v_r}{\partial \theta^2} - \frac{2}{r^2}\frac{\partial v_\theta}{\partial \theta} + \frac{\partial^2 v_r}{\partial z^2} \right] + \rho g_r \\ & = \rho \left(\frac{\partial v_r}{\partial t} + v_r \frac{\partial v_r}{\partial r} + \frac{v_\theta}{r}\frac{\partial v_r}{\partial \theta} - \frac{v_\theta^2}{r} + v_z \frac{\partial v_r}{\partial z} \right), \end{aligned} \tag{9.59}$$

$$\begin{aligned} \hat{\boldsymbol{e}}_\theta: \quad & -\frac{1}{r}\frac{\partial p}{\partial \theta} + \mu \left[\frac{\partial}{\partial r}\left(\frac{1}{r}\frac{\partial (rv_\theta)}{\partial r} \right) + \frac{1}{r^2}\frac{\partial^2 v_\theta}{\partial \theta^2} + \frac{2}{r^2}\frac{\partial v_r}{\partial \theta} + \frac{\partial^2 v_\theta}{\partial z^2} \right] + \rho g_\theta \\ & = \rho \left(\frac{\partial v_\theta}{\partial t} + v_r \frac{\partial v_\theta}{\partial r} + \frac{v_\theta}{r}\frac{\partial v_\theta}{\partial \theta} + \frac{v_r v_\theta}{r} + v_z \frac{\partial v_\theta}{\partial z} \right), \end{aligned} \tag{9.60}$$

$$\hat{\boldsymbol{e}}_z: \quad -\frac{\partial p}{\partial z}+\mu\left[\frac{1}{r}\frac{\partial}{\partial r}\left(r\frac{\partial v_z}{\partial r}\right)+\frac{1}{r^2}\frac{\partial^2 v_z}{\partial \theta^2}+\frac{\partial^2 v_z}{\partial z^2}\right]+\rho g_z$$
$$=\rho\left(\frac{\partial v_z}{\partial t}+v_r\frac{\partial v_z}{\partial r}+\frac{v_\theta}{r}\frac{\partial v_z}{\partial \theta}+v_z\frac{\partial v_z}{\partial z}\right). \tag{9.61}$$

Canceling out terms using the above assumptions (do it, using the worksheet from Sect. 8.7), we are left with

$$-\frac{\partial p}{\partial r}=-\rho\frac{v_\theta^2}{r} \quad \text{and} \quad \mu\frac{\partial}{\partial r}\left(\frac{1}{r}\frac{\partial (rv_\theta)}{\partial r}\right)=0. \tag{9.62}$$

These two governing differential equations of motion are decoupled (i.e., we can solve v_θ from the second equation and then p from the first equation rather than having to solve simultaneously two equations for two unknowns); hence, let us solve them sequentially. Integrating the second equation and putting it in the form of d(something)/dr as suggested in Appendix 8 of Chap. 8, we obtain

$$\int\frac{\partial}{\partial r}\left(\frac{1}{r}\frac{\partial}{\partial r}(rv_\theta)\right)dr=\int 0\,dr \rightarrow \frac{1}{r}\frac{\partial}{\partial r}(rv_\theta)=c_2. \tag{9.63}$$

Multiplying through by r and integrating again, we have

$$\int\frac{\partial}{\partial r}(rv_\theta)\,dr=\int rc_2\,dr \rightarrow rv_\theta=\frac{c_2}{2}r^2+c_3, \tag{9.64}$$

or

$$v_\theta(r)=\frac{c_2}{2}r+\frac{c_3}{r}. \tag{9.65}$$

The no-slip condition at the inner cylinder, which may rotate at angular velocity ω_a, is $v_\theta(r=a)=a\omega_a$ (remember, ω has units of inverse time); likewise, the no-slip condition at the outer cylinder, which may rotate at angular velocity ω_b, is $v_\theta(r=b)=b\omega_b$. Hence, we have

$$a\omega_a=\frac{c_2}{2}a+\frac{c_3}{a}, \quad b\omega_b=\frac{c_2}{2}b+\frac{c_3}{b}, \tag{9.66}$$

which are simply two algebraic equations in terms of two unknowns. Solving these two equations simultaneously, we find that

$$c_2 = \frac{2\left(b^2\omega_b - a^2\omega_a\right)}{b^2 - a^2}, \quad c_3 = \frac{a^2b^2(\omega_a - \omega_b)}{b^2 - a^2}. \tag{9.67}$$

Thus, the velocity field is $\boldsymbol{v} = v_\theta(r)\hat{\boldsymbol{e}}_\theta$, where

$$v_\theta(r) = \left(\frac{b^2\omega_b - a^2\omega_a}{b^2 - a^2}\right)r + \left(\frac{a^2b^2(\omega_a - \omega_b)}{b^2 - a^2}\right)\frac{1}{r}. \tag{9.68}$$

Again, check that the boundary conditions are enforced at $r = a$ and $r = b$. Given this "general" solution, it is useful to consider numerous special cases. For example, if we rotate the cylinders at the same angular velocity (i.e., let $\omega_a = \omega_b = \omega$), then

$$v_\theta(r) = r\omega; \tag{9.69}$$

that is, when the angular velocities are the same, in magnitude and direction, the fluid moves like a rigid body. Question: What is the associated vorticity? Recalling Eq. (7.43), $\boldsymbol{\zeta} = \nabla \times \boldsymbol{v} = 2\omega\hat{\boldsymbol{e}}_z$ as we would expect. Hence, this flow is not irrotational.

Recalling that many cells are very sensitive to imposed shear stresses, note that NASA sought to minimize flow-induced shear in their aforementioned bioreactor so that the effects of the simulated microgravity could be isolated and studied separately. Recall, therefore, that for Newtonian fluids [cf. Eqs. (7.64) and (7.58)],

$$\sigma_{r\theta} = \mu\left[r\frac{\partial}{\partial r}\left(\frac{v_\theta}{r}\right) + \frac{1}{r}\frac{\partial v_r}{\partial \theta}\right], \tag{9.70}$$

where $v_r \equiv 0$ here and, thus,

$$\sigma_{r\theta} = \mu r\frac{\partial}{\partial r}\left(\frac{v_\theta}{r}\right). \tag{9.71}$$

To find the shear stress at any point in the fluid, including at the walls, we know from Eq. (9.69) that $v_\theta = r\omega$ if the cylinders rotate at the same angular velocity. In this case, then, the shear stress is

$$\sigma_{r\theta} = \mu r\frac{\partial}{\partial r}(\omega) = 0 \tag{9.72}$$

because ω is not a function of r. Hence, rotating the fluid as a rigid-body results in a shearless flow as desired by NASA. Clearly, the design of both

the device and the experimental protocol is possible only through a fluid mechanical analysis.

Observation 9.2. Although our analysis of the NASA bioreactor gives us a good "feel" for the fluid mechanics, actual research has been based on a more general mathematical analysis. For example, Tsao et al. (1994) considered a bioreactor having dimensions $a = 2.86$ cm, $b = 4.0$ cm, and length (height) $h = 11$ cm. For a Newtonian fluid of mass density $\rho = 1{,}020$ kg/m^3 and viscosity $\mu = 0.97$ cP $= 0.97 \times 10^{-3}$Ns/m^2, they showed that two secondary flows (cf. Fig. 8.12) occur in addition to the primary circumferential flow; that is, assuming only a steady, axisymmetric flow, the numerical solution of the mass balance and Navier–Stokes equations reveals a counterclockwise circulation and an opposing clockwise circulation pattern in the r-z plane; that is, both v_r and v_z are nonzero, in general, in the actual bioreactor wherein $h = 11$ cm is much larger than the gap $b - a = 1.14$ cm. They suggest that these countercirculation patterns facilitate good mixing, which enables oxygen and nutrient transport to free-floating cells. The numerical details are beyond the present scope, however, and the interested reader is referred to the original paper.

9.3.3 Viscometer Application

Recall that an incompressible, Newtonian fluid is characterized by a single material parameter, the viscosity μ (Fig. 7.11). Fundamental to the solution of Newtonian flows, therefore, is determination of the numerical value of μ for the fluid of interest and under the conditions of interest. For example, the viscosity of many Newtonian fluids varies strongly with temperature (e.g., motor oil is much more viscous at low temperatures); indeed, this relationship is often approximated via $\log \mu = \log A + 0.434B/\mathrm{T}$, where A and B are material parameters and T is temperature (i.e., $\mu = Ae^{B/T}$).

There are numerous ways to determine the value of μ for a Newtonian fluid. Devices designed specifically for such experimental determinations are called viscous meters or *viscometers*. Common designs of viscometers are the capillary-tube, the falling-sphere, the cone-and-plate, and the concentric-cylinder viscometer. In a falling-sphere viscometer, one measures the time of descent of a solid sphere in a column of fluid of interest. This situation can be modeled as the flow of a fluid around a stationary sphere. Under conditions wherein the viscous effects are much greater than the inertial effects, the Navier–Stokes equations simplify and one obtains a solution (Slattery 1981) that allows the viscosity to be inferred from the mass and diameter of the (smooth) sphere and the descent time

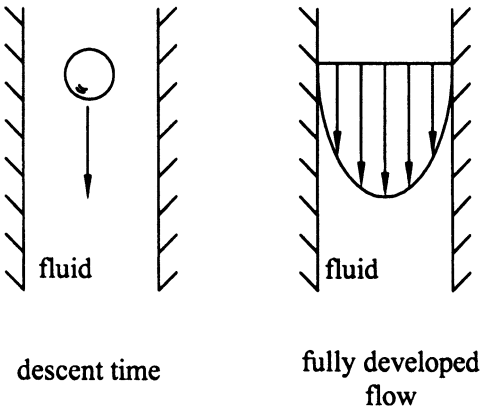

FIGURE 9.15 Schema of two additional setups that are used as viscometers (cf. Fig. 7.16).

over a prescribed length of travel (Fig. 9.15). This is discussed further in Chap. 10 using a nondimensional approach.

In the cone-and-plate viscometer, one measures the torque T that is necessary to rotate a small-angle cone at a specified angular velocity within a fluid of interest (Fig. 7.16; see, e.g., Slattery, 1981). Such devices have been used commonly to quantify the viscosity of blood as well as to subject cultured monolayers of cells to known shear stresses. An approximate relation among the torque, viscosity, and device parameters is given in Sect. 7.6. Let us now consider an exact solution for the concentric-cylinder device based on the general solution found in the previous section.

In the concentric-cylinder viscometer, one likewise measures the torque needed to rotate the inner cylinder at a constant angular velocity. Specifically, if we fix the outer cylinder ($\omega_b = 0$) and only rotate the inner cylinder at ($\omega_a \equiv \omega$) then Eq. (9.68) reduces to

$$v_\theta(r) = \frac{a^2\omega}{b^2 - a^2}\left(\frac{b^2}{r} - r\right). \tag{9.73}$$

Now, the torque (or twisting moment) T is, of course, a force acting at a distance. In particular, for the inner cylinder, we have

$$\sum M_z\big)_0 = 0 \rightarrow T - \int_A a\tau_w dA = 0, \tag{9.74}$$

where $\tau_w dA$ is the differential force acting at distance a from the centerline (Fig. 9.16), the torque being balanced by all such differential torques. Clearly, we need to compute the wall shear stress τ_w on the inner cylinder, which is equal and opposite $\sigma_{r\theta}$ in the fluid at $r = a$. From Eq. (9.73) and the constitutive relation for the fluid [Eq. (7.64)], we have

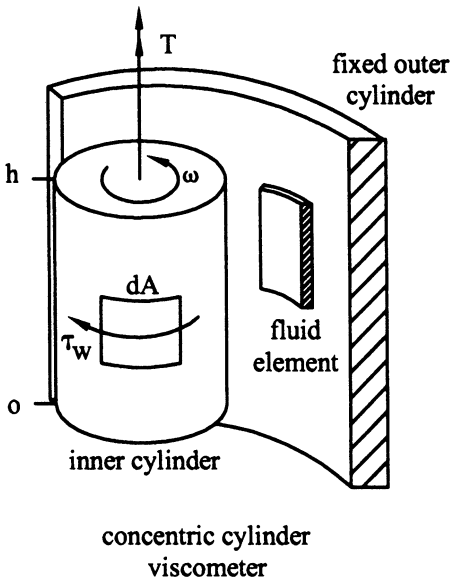

FIGURE 9.16 Detail of the wall shear stresses τ_w that act on the inner cylinder of the concentric-cylinder viscometer. The applied torque T must balance these stresses in a steady-state situation.

$$\sigma_{r\theta} = \mu r \frac{\partial}{\partial r}\left(\frac{v_\theta}{r}\right) = \mu r \frac{\partial}{\partial r}\left[\frac{a^2\omega}{b^2 - a^2}\left(\frac{b^2}{r^2} - 1\right)\right]. \tag{9.75}$$

Thus, the shear stress at any point r is

$$\sigma_{r\theta} = \mu r\left[\frac{a^2\omega}{b^2 - a^2}\left(-\frac{2b^2}{r^3}\right)\right] \rightarrow \sigma_{r\theta} = -\frac{2\mu b^2 a^2 \omega}{b^2 - a^2}\left(\frac{1}{r^2}\right); \tag{9.76}$$

the negative sign reveals a direction opposite that for a positive sign convention. To find the shear stress on the wall, we need to calculate $\sigma_{r\theta}$ at $r = a$, which is

$$\sigma_{r\theta}(r = a) = -\frac{2\mu b^2 \omega}{b^2 - a^2}. \tag{9.77}$$

Because $b > a$, the shear stress $\sigma_{r\theta}$ is negative on an inner (negative) face of the fluid, and the free-body diagram for the inner cylinder in terms of τ_w is as shown in Fig. 9.16. The shear stress on the wall is thus

$$\tau_w = |\sigma_{r\theta}(r = a)| = \frac{2\mu b^2 \omega}{b^2 - a^2}, \tag{9.78}$$

in the direction shown.

With the differential area $dA = dz\ ad\theta$ (where $r = a$), Eq. (9.74) becomes

$$T = \int_0^h \int_0^{2\pi} a^2 \tau_w d\theta dz = \frac{2\mu b^2 \omega}{b^2 - a^2} \left(a^2\right) \int_0^h \int_0^{2\pi} d\theta dz, \tag{9.79}$$

or

$$T = \frac{4\pi\mu a^2 b^2 \omega h}{b^2 - a^2}. \tag{9.80}$$

Hence, the viscosity μ can be "measured" (actually inferred) by measuring the geometry (a, b, h), angular speed (ω), and applied torque T, namely

$$\mu = \frac{T\left(b^2 - a^2\right)}{4\pi a^2 b^2 h \omega}. \tag{9.81}$$

Again, therefore, we see that analysis allows one to design an experiment (i.e., to determine what to measure, why, and to what resolution).

It should be noted that many concentric cylinder viscometers have a small gap distance ($b - a$) relative to the inner radius a. Although Eq. (9.81) should be used to compute μ, it is interesting to note that when $b - a \ll a$, we can think of the problem locally as a "flat" (inner) plate moving relative to an "outer" stationary one. In this case, we can exploit the solution in Example 9.2 for the Couette flow. In that case, $U_0 = a\omega$ and $h = b - a$, and the associated shear stress is

$$\sigma_{xy} = \frac{\mu a \omega}{b - a} \rightarrow \tau_w = \left|\frac{\mu a \omega}{b - a}\right|. \tag{9.82}$$

The associated torque is thus

$$T = \int\int \tau_w a dA = \frac{\mu a^2 \omega}{b - a}(2\pi a h) \rightarrow \mu = \frac{T(b - a)}{2\pi a^3 \omega h}. \tag{9.83}$$

Calling this solution for the viscosity μ_{approx} and Eq. (9.81) μ_{exact}, note that the error due to the flat plate assumption is

$$\text{error} = \frac{\mu_{\text{approx}} - \mu_{\text{exact}}}{\mu_{\text{exact}}} = \frac{2b^2 - (ab + a^2)}{ab + a^2}. \tag{9.84}$$

Note: Viscosity has units of N s/m^2 in the SI system, but values are sometimes reported as Poise (P) or centiPoise (cP). The conversion is 1 P = 0.1 N s/m^2 or 1 cP = 1×10^{-3} N s/m^2; alternatively, 1 P = 1 dyn s/cm^2 = 1 g/cm s.

Example 9.5 In an experiment, one has

$$a = 9\,\text{mm}, \quad b = 9.2\,\text{mm}, \quad \omega = 1{,}200\,\text{rpm},$$
$$h = 60\,\text{mm}, \quad T = 0.0036\,\text{N m}.$$

Compute the error in "measuring" μ based on the flat plate assumption.

Solution: Based on the exact solution

$$\mu_{\text{exact}} = \frac{(0.0036)\left(0.0092^2 - 0.009^2\right)}{4\pi(0.009)^2(0.0092)^2(0.06)(125.66)} = 0.02017\,\frac{\text{N s}}{\text{m}^2},$$

where $\omega = (1{,}200\ \text{rpm})(1\ \text{min}/60\ \text{s})(2\ \pi\text{rad/rev}) = 125.66$ rad/s, whereas, based on the approximate solution,

$$\mu_{\text{approx}} = \frac{T(b-a)}{2\pi a^3 \omega h} = \frac{0.0036(0.0002)}{2\pi(0.009)^3(125.66)(0.06)} = 0.02085\,\frac{\text{N s}}{\text{m}^2}$$

Hence, our error is only

$$\text{error} = \frac{\mu_{\text{approx}} - \mu_{\text{exact}}}{\mu_{\text{exact}}} = \frac{0.02085 - 0.02017}{0.02017} = 3.37\%.$$

Indeed, from our general formula [Eq. (9.84)],

$$\text{error} = \frac{2(0.0092)^2 - \left((0.009)(0.0092) + (0.009)^2\right)}{(0.009)(0.0092) + (0.009)^2} = 3.35\%,$$

the difference being due to numerical round-off errors.

9.4 Steady Flow in an Elliptical Cross Section

9.4.1 Biological Motivation

Many blood vessels are embedded within a particular soft tissue. Examples include the arteries within muscular organs such as the diaphragm, heart, uterus, and skeletal muscle. It is easy to imagine, therefore, that as the surrounding tissue deforms, the cross section of the embedded vessel can likewise change (Fig. 9.17). For example, blood vessels in the heart are compressed by the

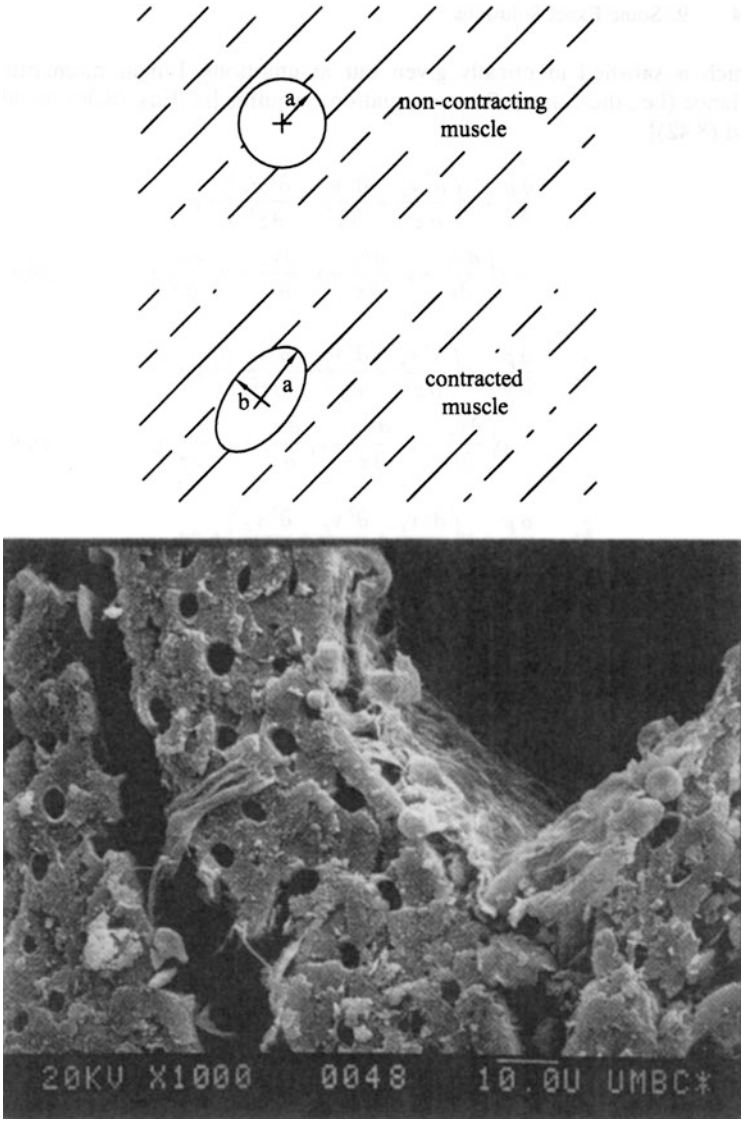

FIGURE 9.17 Illustration (*upper*) that many blood vessels are contained within surrounding soft tissue and that the deformation of the tissue can alter the cross-sectional shape of the vessel. Shown, too, is a scanning electron micrograph of heart tissue (*lower*): The many small holes are capillaries and the large hole is an artery. Note the contiguous endothelial cell layer inside the artery and the remnant red blood cells (biconcave disks about 8 μm in diameter) around the opening of the artery. It is easy to imagine that the cross sections of each of these vessels can be altered significantly by the finite strains experienced by the wall of the heart (recall Fig. 2.19).

contracting muscle; indeed, vessels in the left heart are compressed closed during systole, which is why the left heart is perfused during diastole. There is a need, therefore, to consider flows in noncircular geometries. Here, let us consider a steady flow within a tube of elliptical cross section, defined by major and minor radii a and b, respectively.

9.4.2 Mathematical Formulation

Let the z axis go through the center of the elliptical cross section with a boundary given by $x^2/a^2 + y^2/b^2 = 1$. Moreover, similar to our analysis of flow through the cylindrical tube, let us assume the following:

1. Newtonian fluid ($\mu = \text{constant}$)
2. Incompressible flow ($\nabla \cdot \boldsymbol{v} = 0$)
3. Steady flow ($\partial \boldsymbol{v}/\partial t = \boldsymbol{0}$)
4. Axial flow ($v_x = v_y = 0$)
5. Negligible body forces ($\boldsymbol{g} = \boldsymbol{0}$)
6. Fully developed flow ($\partial \boldsymbol{v}/\partial z = \boldsymbol{0}$)
7. Laminar flow

To solve this problem using the Navier–Stokes equation, we have two choices: use elliptical coordinates or use Cartesian coordinates. We choose the latter here. Because of the no-slip boundary condition, the velocity $\boldsymbol{v} = v_z(x, y)\hat{\boldsymbol{e}}_z$ must be zero at all x and y around the inner surface of the ellipse. This will play a key role in our solution. First, however, recall that mass balance requires

$$\frac{\partial v_x}{\partial x} + \frac{\partial v_y}{\partial y} + \frac{\partial v_z}{\partial z} = 0, \tag{9.85}$$

which is satisfied identically given our assumptions. Linear momentum balance (i.e., the Navier–Stokes equation) requires [cf. Eqs. (8.36), (8.40), and (8.42)]

$$\begin{aligned} \hat{\boldsymbol{i}}: \quad & -\frac{\partial p}{\partial x} + \mu\left(\frac{\partial^2 v_x}{\partial x^2} + \frac{\partial^2 v_x}{\partial y^2} + \frac{\partial^2 v_x}{\partial z^2}\right) + \rho g_x \\ & = \rho\left(\frac{\partial v_x}{\partial t} + v_x\frac{\partial v_x}{\partial x} + v_y\frac{\partial v_x}{\partial y} + v_z\frac{\partial v_x}{\partial z}\right), \end{aligned} \tag{9.86}$$

$$\begin{aligned} \hat{\boldsymbol{j}}: \quad & -\frac{\partial p}{\partial y} + \mu\left(\frac{\partial^2 v_y}{\partial x^2} + \frac{\partial^2 v_y}{\partial y^2} + \frac{\partial^2 v_y}{\partial z^2}\right) + \rho g_y \\ & = \rho\left(\frac{\partial v_y}{\partial t} + v_x\frac{\partial v_y}{\partial x} + v_y\frac{\partial v_y}{\partial y} + v_z\frac{\partial v_y}{\partial z}\right), \end{aligned} \tag{9.87}$$

$$\hat{\boldsymbol{k}}: \quad -\frac{\partial p}{\partial z}+\mu\left(\frac{\partial^2 v_z}{\partial x^2}+\frac{\partial^2 v_z}{\partial y^2}+\frac{\partial^2 v_z}{\partial z^2}\right)+\rho g_z = \rho\left(\frac{\partial v_z}{\partial t}+v_x\frac{\partial v_z}{\partial x}+v_y\frac{\partial v_z}{\partial y}+v_z\frac{\partial v_z}{\partial z}\right). \tag{9.88}$$

After canceling out terms consistent with the above assumptions (do it using the worksheets in Sect. 8.7), we are left with

$$-\frac{\partial p}{\partial x}=0, \quad -\frac{\partial p}{\partial y}=0, \quad -\frac{\partial p}{\partial z}+\mu\left(\frac{\partial^2 v_z}{\partial x^2}+\frac{\partial^2 v_z}{\partial y^2}\right)=0. \tag{9.89}$$

The first and second of these equations show that the pressure is a function of z at most, similar to the solution for a cylindrical tube. Because the velocity is a function of x and y at most, both the pressure gradient and the viscous term must equal a constant. Thus, our governing differential equation is

$$\frac{1}{\mu}\frac{dp}{dz}=\frac{\partial^2 v_z}{\partial x^2}+\frac{\partial^2 v_z}{\partial y^2}. \tag{9.90}$$

To solve this problem, one could first seek a solution to the homogenous differential equation of the form[1]

$$\frac{\partial^2 v_z}{\partial x^2}+\frac{\partial^2 v_z}{\partial y^2}=0. \tag{9.91}$$

Although there are many different approaches to solve this linear partial differential equation, here we shall consider a very simple, yet powerful approach to solve the full nonhomogeneous equation. Note that the full solution v_z must satisfy the no-slip boundary condition around the inner perimeter. Consequently, let us consider a function $g(x,y)$ that is zero over the entire boundary of the flow, which for the elliptical boundary is $x^2/a^2+y^2/b^2-1=0$. Hence, as a trial solution (i.e., guess), let

$$v_z(x,y)=cg(x,y)=c\left(\frac{x^2}{a^2}+\frac{y^2}{b^2}-1\right), \tag{9.92}$$

where c is a yet unknown parameter. Taking the partial derivatives with respect to x, we get

[1] One may recognize that this is a 2-D Laplace equation, written as $\nabla^2 v_z=0$, which appears widely in physics.

$$\frac{\partial v_z}{\partial x} = c\frac{2x}{a^2} \quad \text{and} \quad \frac{\partial^2 v_z}{\partial x^2} = c\frac{2}{a^2}, \tag{9.93}$$

and similarly taking the partial derivatives with respect to y, we get

$$\frac{\partial v_z}{\partial y} = c\frac{2y}{b^2} \quad \text{and} \quad \frac{\partial^2 v_z}{\partial y^2} = c\frac{2}{b^2}. \tag{9.94}$$

Substituting these relations into the governing differential equation and solving for c, we obtain

$$c\left(\frac{2}{a^2}\right) + c\left(\frac{2}{b^2}\right) = \frac{1}{\mu}\frac{dp}{dz} \rightarrow c = \frac{1}{2\mu}\frac{dp}{dz}\left(\frac{a^2b^2}{a^2+b^2}\right). \tag{9.95}$$

Substituting this expression into Eq. (9.92), we get the following solution for the velocity field:

$$v_z(x,y) = \frac{1}{2\mu}\frac{dp}{dz}\left(\frac{a^2b^2}{a^2+b^2}\right)\left(\frac{x^2}{a^2}+\frac{y^2}{b^2}-1\right), \tag{9.96}$$

which satisfies both the differential equation and the boundary conditions. Because the governing equations are linear, this trial solution is THE solution (i.e., mathematicians have proved uniqueness theorems for such linear differential equations). Note, too, that if $b = a$, with $x^2 + y^2 = r^2$, we recover the solution for the circular tube [cf. Eq. (9.45)], as we should. Such checks provide added confidence in the formulation and solution of the problem. Finally, given solutions for the pressure and velocity fields, other quantities of interest are calculated easily as in prior sections. This is left as an exercise.

9.5 Pulsatile Flow

Of the assumptions invoked in Sect. 9.2, the most suspect for many biological problems is that of steady flow. Here, therefore, let us consider an analysis of pulsatile flows based on a solution by J. R. Womersley in the 1950s. Because of the additional complexity due to the pulsatility, this shall return us to the Navier–Stokes solution for flow in a cylindrical rigid tube.

9.5.1 Some Biological Motivation

The cardiac cycle consists of four primary phases: diastolic filling, isovolumetric contraction, ejection, and isovolumetric relaxation (Fig. 9.18, top), which

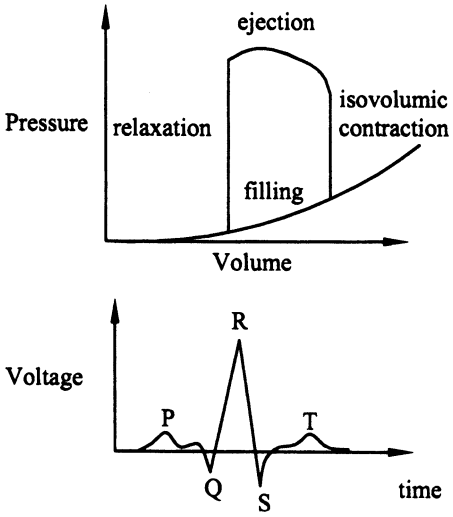

FIGURE 9.18 Schematic illustration of the four phases of the cardiac cycle: diastolic filling, isovolumic contraction (which builds up the ventricular pressure), ejection, and isovolumic relaxation. These mechanical phases are controlled by the electrical activity of the heart, which is monitored easily with an electrocardiogram (or EKG). This reminds us that coupled effects such as electromechanics are very important, as noted in Sect. 11.6.

corresponds to the primary electrical events in the heart as revealed by an electrocardiogram (Fig. 9.18, bottom). As a result, the heart is a "pulsatile pump" and the associated flow within the arterial tree is pulsatile. Figure 9.19 shows, for example, the pressure P history in a typical artery (see Fig. 8.14 for data on the flow); each can be described well by a Fourier series (Milnor, 1989). For example, the pressure waveform for an aortic flow can be described by

$$p(t) = p_m + \sum_{n=1}^{N} (A_n \cos n\omega t + B_n \sin n\omega t), \tag{9.97}$$

where p_m is the mean pressure, ω is the fundamental (circular) frequency, and A_n and B_n are the Fourier coefficients for N harmonics. Table 9.1 lists typical values.

9.5.2 *Mathematical Formulation*

Womersley suggested that the pulsatile axial flow of an incompressible Newtonian fluid in a rigid tube could be studied by assuming that the pressure

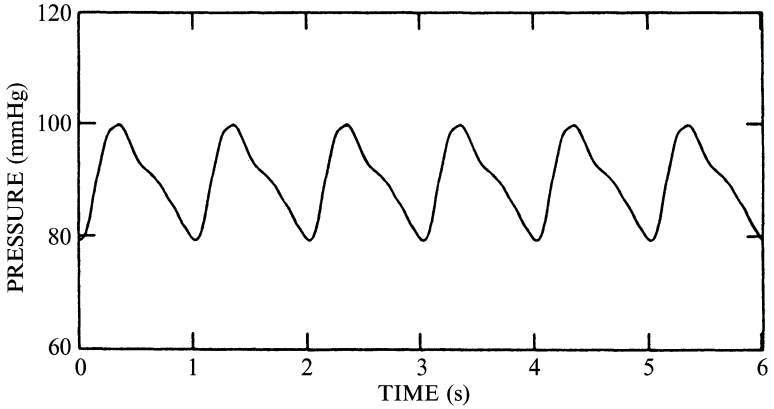

FIGURE 9.19 Typical variations in arterial pressures over the cardiac cycle, which can be described well via a Fourier series representation.

TABLE 9.1 Values of the Fourier coefficients for a Fourier series representation of an aortic pressure.

	$n=1$	$n=2$	$n=3$	$n=4$	$n=5$	$n=6$	$n=7$
Pressure C_n	18.6	8.6	5.1	2.9	1.3	1.4	1.2
Pressure Φ_n	−1.67	−2.25	−2.61	−3.12	−2.91	−2.81	2.93
Flow C_n	202	157	103	62	47	42	31
Flow Φ_n	−0.78	−1.50	−2.11	−2.46	−2.59	−2.91	2.92

Note. The modulus $C_n = \sqrt{A_n^2 + B_n^2}$, in mmHg or mL/s, whereas the phase $\Phi_n = \tan^{-1}(B_n/A_n)$, in radians, for each harmonic n. The mean values are $P_m = 85$ mmHg and $Q_m = 110$ mL/s, with a fundamental frequency of 1.25 Hz
Source. From Milnor (1989)

gradient $\partial p/\partial z$ could likewise be described by multiple harmonics. Consequently, he suggested that we let

$$\frac{\partial p}{\partial z} = \phi_0 + \sum_{n=1}^{N} (\phi_n \cos n\omega t + \psi_n \sin n\omega t), \tag{9.98}$$

where ϕ_0 is the mean (steady) portion of the pressure gradient and ϕ_n and ψ_n are Fourier coefficients for the nth harmonic. For analytical expediency, however, note that if $\Psi = \phi - i\psi$, where $i = \sqrt{-1}$, then

$$\begin{aligned} \Psi e^{i\omega t} &= (\phi - i\psi)(\cos \omega t + i \sin \omega t) \\ &= \phi \cos \omega t + \psi \sin \omega t + i(\phi \sin \omega t - \psi \cos \omega t). \end{aligned} \tag{9.99}$$

Hence, if we take the real part

$$\mathrm{Re}\left(\Psi e^{i\omega t}\right) = \phi \cos \omega t + \psi \sin \omega t, \tag{9.100}$$

we obtain terms that appear in the Fourier representation of Eq. (9.98). (Note: Do not confuse the real part of a complex function Re() with the Reynolds' number Re). In particular, we can now let

$$\frac{\partial p}{\partial z} = \phi_0 + \sum_{n=1}^{N} \mathrm{Re}\left(\Psi_n e^{in\omega t}\right), \tag{9.101}$$

which is simply a compact way to represent the assumed variation in the pressure gradient.

Recall from Eq. (9.38), therefore, that for steady flow in a circular tube, the Navier–Stokes equation reduces to

$$\frac{dp}{dz} = \mu\left[\frac{1}{r}\frac{\partial}{\partial r}\left(r\frac{\partial v_z}{\partial r}\right)\right]. \tag{9.102}$$

The assumptions under which this flow takes place are essentially the same for the pulsatile flow that we are considering, with the exception that the assumption of steady flow does not apply. Again, therefore, mass balance [Eq. (9.34)] is satisfied identically for a $\boldsymbol{v} = v_z(r,t)\hat{\boldsymbol{e}}_z$, and the Navier–Stokes equations [Eqs. (9.35)–(9.37)] reduce to

$$-\frac{\partial p}{\partial r} = 0, \quad -\frac{\partial p}{\partial \theta} = 0, \quad -\frac{\partial p}{\partial z} + \mu\left[\frac{1}{r}\frac{\partial}{\partial r}\left(r\frac{\partial v_z}{\partial r}\right)\right] = \rho\frac{\partial v_z}{\partial t}. \tag{9.103}$$

The first two equations show that the pressure must be a function of z and time at most: $p = p(z, t)$. Hence, the single governing differential equation is

$$\rho\frac{\partial v_z(r,t)}{\partial t} + \frac{\partial p(z,t)}{\partial z} = \mu\left[\frac{1}{r}\frac{\partial}{\partial r}\left(r\frac{\partial v_z(r,t)}{\partial r}\right)\right]. \tag{9.104}$$

Note that Eq. (9.104) is linear in both the pressure $p(z, t)$ and velocity $v_z(r, t)$ and, therefore, solutions of this linear differential equation can be superimposed. Let us deal with the steady and unsteady parts of the flow independently. This is a very important observation because the steady part of the flow has already been solved in Sect. 9.2. Thus, here we simply need to consider the unsteady part.

To look at the steady and unsteady parts of the flow separately, let the subscripts s and u denote steady flow and unsteady flow, respectively. Thus, we can write the unknown pressure and velocity fields as

$$p(z,t) = p_s(z) + p_u(z,t) \quad \text{and} \quad v_z(r,t) = v_s(r) + v_u(r,t). \tag{9.105}$$

Substituting these into Eq. (9.104), we obtain

$$\begin{aligned}\left\{\frac{\partial p_s(z)}{\partial z} - \mu\left[\frac{1}{r}\frac{\partial}{\partial r}\left(r\frac{\partial v_s(r)}{\partial r}\right)\right]\right\} + \left\{\rho\frac{\partial v_u(r,t)}{\partial t} + \frac{\partial p_u(z,t)}{\partial z}\right.\\ \left. -\mu\left[\frac{1}{r}\frac{\partial}{\partial r}\left(r\frac{\partial v_u(r,t)}{\partial r}\right)\right]\right\} = 0\end{aligned} \tag{9.106}$$

wherein we grouped terms that depend on time separate from those that do not. Because of the differences between the two groups of terms, each group must equal zero separately. The former is simply that which was solved in Sect. 9.2; hence, v_s is known. Let us focus our attention on the governing equation for the unsteady part of the flow, namely

$$\rho\frac{\partial v_u}{\partial t} + \frac{\partial p_u}{\partial z} - \mu\left[\frac{1}{r}\frac{\partial}{\partial r}\left(r\frac{\partial v_u}{\partial r}\right)\right] = 0. \tag{9.107}$$

Similar to the steady-flow solution, let us assume that the pressure gradient does not depend on z in a fully developed flow. Hence, the pulsatile pressure gradient depends on time t only, as given by Eq. 9.101.

Moreover, because of the linearity of the governing equation, let us solve Eq. (9.107) separately for each harmonic n (=1,2, ..., N). Our governing equation for unsteady flow thus becomes

$$\mu\left[\frac{1}{r}\frac{\partial}{\partial r}\left(r\frac{\partial v_u}{\partial r}\right)\right] - \rho\frac{\partial v_u}{\partial t} = \Psi_n e^{in\omega t} \tag{9.108}$$

for *each* n. Using separation of variables, we can separate the equation for $v_u(r, t)$ into one part that depends on r only and another that depends on t only; that is, let

$$v_u(r,t) = V_n(r)e^{in\omega t} \tag{9.109}$$

for each n. Substituting this equation into Eq. (9.108), we obtain

$$\mu\left[\frac{1}{r}\frac{\partial}{\partial r}\left(r\frac{\partial}{\partial r}\left[V_n(r)e^{in\omega t}\right]\right)\right] - \rho\frac{\partial}{\partial t}\left[V_n(r)e^{in\omega t}\right] = \Psi_n e^{in\omega t} \tag{9.110}$$

The common term $e^{in\omega t}$ cancels throughout, leaving the ordinary differential equation

$$\frac{d^2V_n}{dr^2}+\frac{1}{r}\frac{dV_n}{dr}-\frac{\rho}{\mu}(in\omega)V_n=\frac{1}{\mu}\Psi_n \tag{9.111}$$

for each harmonic n. Thus, our governing ordinary differential equation for each n (now suppressed notationally) becomes

$$\frac{d^2V}{dr^2}+\frac{1}{r}\frac{dV}{dr}+\lambda^2V=\frac{\Psi}{\mu}, \tag{9.112}$$

where $\lambda^2\equiv i^3n\omega\rho/\mu$. This governing differential equation has the form of a standard Bessel's equation

$$\frac{d^2y}{dx^2}+\frac{1}{x}\frac{dy}{dx}+y=0, \tag{9.113}$$

which has a solution of the form

$$y(x)=c_1J_0(x)+c_2Y_0(x), \tag{9.114}$$

where $J_0(x)$ and $Y_0(x)$ are Bessel functions of order zero and the first and second kinds, respectively. For example,

$$J_0(x)=1-\frac{x^2}{2^2}+\frac{x^4}{2^24^2}-\frac{x^6}{2^24^26^2}+\ldots, \tag{9.115}$$

$$Y_0(x)=J_0(x)\log(x)+\frac{x^2}{4}-\frac{3x^4}{128}+\ldots. \tag{9.116}$$

Now, if we consider a change of variables, $x\equiv\lambda z$, then

$$\frac{d}{dx}=\left(\frac{d}{dz}\right)\left(\frac{dz}{dx}\right)=\frac{1}{\lambda}\frac{d}{dz}\quad\text{and}\quad\frac{d^2}{dx^2}=\frac{1}{\lambda}\frac{d}{dz}\left(\frac{1}{\lambda}\frac{d}{dz}\right)=\frac{1}{\lambda^2}\frac{d^2}{dz^2}, \tag{9.117}$$

thus, an equation of the form

$$\frac{d^2y}{dz^2}+\frac{1}{z}\frac{dy}{dz}+\lambda^2y=0 \tag{9.118}$$

admits a solution of the form (cf. Eq. 9.112)

$$y(z)=c_1J_0(\lambda z)+c_2Y_0(\lambda z). \tag{9.119}$$

The homogeneous solution of our governing equation (9.112) is thus

$$V_H(r) = c_1 J_0(\lambda r) + c_2 Y_0(\lambda r), \tag{9.120}$$

where c_2 must be zero to maintain $V(r)$ finite at the centerline $r = 0$ (a similar restriction was used in the steady-flow solution). For the particular solution, we let $V_p(r) = c_3$ and find that $c_3 = \Psi/\mu\lambda^2$ for each harmonic. Hence,

$$V(r) = V_H(r) + V_p(r) = c_1 J_0(\lambda r) + \frac{\Psi}{\mu\lambda^2} \tag{9.121}$$

for each harmonic n. Now, this solution must satisfy the no-slip boundary condition $v_z(r = a, t) = 0$ for all time and, thus, $V(r = a) = 0$. Hence,

$$c_1 J_0(\lambda a) = -\frac{\Psi}{\mu\lambda^2} \rightarrow c_1 = -\frac{\Psi}{\mu\lambda^2}\left(\frac{1}{J_0(\lambda a)}\right) \tag{9.122}$$

and

$$V(r) = \frac{\Psi}{\mu\lambda^2}\left(1 - \frac{J_0(\lambda r)}{J_0(\lambda a)}\right) \tag{9.123}$$

for each harmonic n. Our final solution, therefore, for the assumed pressure gradient

$$\frac{\partial p}{\partial z}(t) = \frac{\partial p}{\partial z}(\text{steady}) + \sum_{n=1}^{N} \text{Re}\left(\Psi_n e^{in\omega t}\right) \tag{9.124}$$

is

$$v(r,t) = v_s(r) + \text{Re}\left\{\sum_{n=1}^{N}\left[\frac{\Psi_n}{\mu\lambda_n^2}\left(1 - \frac{J_0(\lambda_n r)}{J_0(\lambda_n a)}\right)e^{in\omega t}\right]\right\}, \tag{9.125}$$

where the number of harmonics $n = 1,2,\ldots,N$ is dictated by the Fourier series fit to the pressure gradient data [cf. Eq. (9.98)]. The wall shear stress can thus be computed in the normal way, where

$$\sigma_{rz}(r,t) = \mu\frac{\partial v_z}{\partial r}. \tag{9.126}$$

Note, therefore, that

$$\frac{d}{dx}[J_0(kx)] = -kJ_1(kx), \tag{9.127}$$

where J_1 is a first-order Bessel function of the first kind.

In particular, for each harmonic n, the unsteady contribution is

$$\tau_w)_u = \mathrm{Re}\left\{\frac{|\Psi_n|}{\lambda_n}\left(\frac{J_1(\lambda_n a)}{J_0(\lambda_n a)}\right)e^{in\omega t}\right\}. \tag{9.128}$$

Likewise, the unsteady contribution to the volumetric flow rate is

$$Q_u(t) = \mathrm{Re}\left\{\frac{\pi a^4 \Psi_n e^{in\omega t}}{\mu(\lambda_n a)^2}\left(1 - \frac{2J_1(\lambda_n a)}{\lambda_n a J_0(\lambda_n a)}\right)\right\}. \tag{9.129}$$

Observation 9.3. Computations based on Womersley's results are clearly complex, and the interested reader is referred to Zamir (2000) for more details. Nonetheless, Fig. 9.20 shows velocity profiles (fully developed) at five different times in the cardiac cycle. In particular, note the near-parabolic profiles in the second and fourth panels, but the more blunted profiles in the first, middle, and fifth panels (the first and fifth are the same because the pressure gradient is periodic). Note, too, that we see a flow reversal in the third and fourth panels. Because wall shear stress is proportional to the slope of the velocity profile at the wall (i.e., the velocity gradient), we see that the wall shear stress is oscillatory. There has been considerable attention in the literature on delineating the effects of the oscillatory versus mean wall shear stress on atherogenesis and other pathologies. The interested reader should research this.

Indeed, because of the potential importance of the unsteadiness, a nondimensional parameter called the *Womersley number* α is defined as

$$\alpha = a\sqrt{\frac{\omega\rho}{\mu}}.$$

Typical values in man are $\alpha = 22.2$ in the aorta and $\alpha = 4.0$ in the femoral artery; in comparison, $\alpha = 4.3$ in the rat aorta and $\alpha = 1.5$ in the rat femoral artery. Localization of disease is also correlated with α in some works (see Milnor 1989).

Finally, pulsatility raises important issues with regard to the generation and reflection of waves in distensible tubes. Again, however, the reader is referred to Fung (1984) or Zamir (2000) for more on this advanced topic.

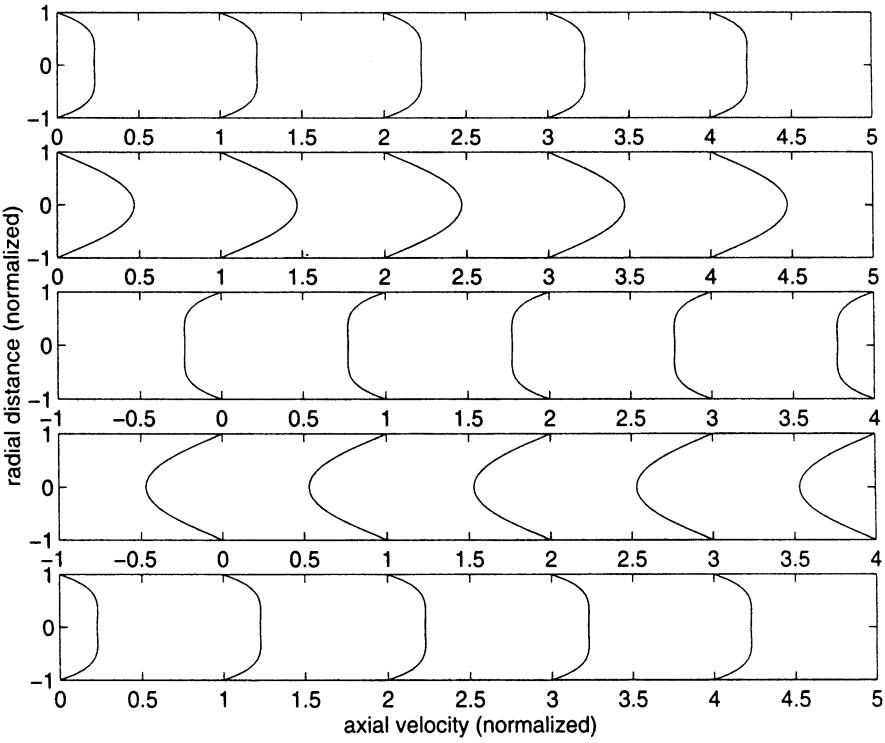

FIGURE 9.20 Pulsatile velocity profiles computed for low frequencies (1 Hz). Results are shown for different phase angles ωt, values being 0° at the top and increasing by 90° for subsequent panels. Note that the flow "develops" over time at a single location similar to its development with distance in an entrance length. [From Zamir (2000), with permission from Springer].

9.6 Non-Newtonian Flow in a Circular Tube

Whereas the flow of air in the airways, the flow of urine in the ureters, and the flow of blood in large arteries at sufficiently high shear rates can all be modeled assuming a Newtonian response, non-Newtonian behavior can be important in the vasculature. Hence, let us consider a brief introduction to an analysis of a relevant non-Newtonian flow.

9.6.1 Motivation

Figure 7.11 shows that blood, among other biological fluids, exhibits a non-Newtonian (pseudoplastic) behavior under certain circumstances (e.g., low shear rates). Whereas quantification of linear (e.g., Newtonian) material

behavior is simplified by the uniqueness of linear relations, quantification of nonlinear behavior remains an area of active research. The interested reader is reminded of Eq. (7.68), but referred to texts on nonlinear rheology (e.g., Tanner, 1985). Here, we shall restrict our attention to the simplest nonlinear behavior—a 1-D power-law model, which is not without mathematical limitations, but does serve to illustrate some nonlinear effects. That is, whereas a 1-D constitutive relation for a Newtonian fluid can be written as

$$\sigma_{rz} = 2\mu D_{rz} = \mu \frac{\partial v_z}{\partial r} \tag{9.130}$$

for an axial flow in a circular tube characterized by $\boldsymbol{v} = v_z(r)\hat{\boldsymbol{e}}_z$ [cf. Eq. (9.45)], a generalization of this relation has been proposed of the form

$$\sigma_{rz} = \underbrace{k\left|\frac{dv_z}{dr}\right|^{n-1}}_{\mu_a} \frac{dv_z}{dr} = k\left(\frac{dv_z}{dr}\right)^n, \tag{9.131}$$

where μ_a is an "apparent" viscosity, k an empirical parameter, and n a nonintegral material parameter. Of course, when $\mu_a \equiv \mu$ and $n = 1$, we recover the Newtonian result. When $n > 1$, we have a dilatant behavior, and when $n < 1$, we have a pseudoplastic behavior (cf. Fig. 7.11). In the special case that $n = 0$, we have $\sigma_{rz} =$ constant, independent of deformation. Such a model is called perfectly plastic in solid mechanics, hence the name pseudoplastic for n approaching zero.

9.6.2 *Mathematical Formulation*

Consider a differential annulus as shown in Fig. 9.21. The sum of the z components of force acting on the full annulus must be zero in the case of a steady flow (i.e., no local acceleration) and without a convective acceleration. Enforcing equilibrium, we have

$$\begin{aligned} p2\pi r\Delta r - \left(p + \frac{\partial p}{\partial z}\Delta z\right)2\pi r\Delta r + \left(\sigma_{rz} + \frac{\partial \sigma_{rz}}{\partial r}\Delta r\right)2\pi(r+\Delta r)\Delta z \\ - \sigma_{rz}2\pi r\Delta z = 0. \end{aligned} \tag{9.132}$$

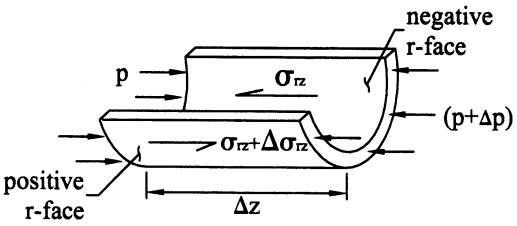

FIGURE 9.21 Free-body diagram of half a differential annulus of fluid and associated shear stresses for purposes of deriving a general equation of motion. Compare to Fig. 8.1 for a cuboidal fluid element.

Simplifying, we have

$$-\frac{\partial p}{\partial z} r\Delta r\Delta z + \frac{\partial \sigma_{rz}}{\partial r} r\Delta r\Delta z + \sigma_{rz}\Delta r\Delta z + \frac{\partial \sigma_{rz}}{\partial r}\Delta r^2\Delta z = 0. \tag{9.133}$$

Dividing this equation by $r\Delta r\Delta z$ and letting $\Delta r \to 0$ and $\Delta z \to 0$, the pressure gradient is found to be [cf. Eq. (8.26)]

$$\frac{\partial p}{\partial z} = \frac{\partial \sigma_{rz}}{\partial r} + \frac{\sigma_{rz}}{r} = \frac{1}{r}\frac{\partial}{\partial r}(r\sigma_{rz}). \tag{9.134}$$

Assuming p varies with z alone and integrating with respect to r yields

$$\int \frac{d}{dr}(r\sigma_{rz})dr = \int \frac{dp}{dz} r\, dr, \tag{9.135}$$

or

$$r\sigma_{rz} = \frac{dp}{dz}\frac{r^2}{2} + c_1 \rightarrow \sigma_{rz} = \frac{dp}{dz}\frac{r}{2} + \frac{c_1}{r}. \tag{9.136}$$

Now, we can apply a constitutive equation for a Newtonian fluid or a non-Newtonian fluid (because this derivation thus far has been independent of the material). For example, substituting the expression for a power-law fluid [Eq. (9.131)] into Eq. (9.136), we obtain

$$k\left(\frac{dv_z}{dr}\right)^n = \frac{dp}{dz}\frac{r}{2} + \frac{c_1}{r}. \tag{9.137}$$

Applying the symmetry condition that $dv_z/dr = 0$ at the centerline ($r = 0$), $c_1 = 0$. Therefore,

$$\left(\frac{dv_z}{dr}\right)^n = \frac{1}{2k}\frac{dp}{dz}r \rightarrow \frac{dv_z}{dr} = \left(\frac{1}{2k}\frac{dp}{dz}\right)^{1/n} r^{1/n}. \tag{9.138}$$

Integrating with respect to r again,

$$\int \frac{d}{dr}(v_z)dr = \left(\frac{1}{2k}\frac{dp}{dz}\right)^{1/n} \int r^{1/n} dr, \tag{9.139}$$

we obtain

$$\begin{aligned} v_z(r) &= \left(\frac{1}{2k}\frac{dp}{dz}\right)^{1/n} \frac{r^{1+1/n}}{1+1/n} + c_2 \\ &\text{or} \\ v_z(r) &= \left(\frac{1}{2k}\frac{dp}{dz}\right)^{1/n} \frac{n}{1+n} r^{(1+n)/n} + c_2. \end{aligned} \tag{9.140}$$

Applying the no-slip boundary condition at the wall, $v_z(r=a)=0$, we find that

$$\begin{aligned} 0 &= \left(\frac{1}{2k}\frac{dp}{dz}\right)^{1/n} \frac{n}{1+n} a^{(1+n)/n} + c_2 \\ &\text{thus} \\ c_2 &= -\left(\frac{1}{2k}\frac{dp}{dz}\right)^{1/n} \frac{n}{1+n} a^{(1+n)/n}. \end{aligned} \tag{9.141}$$

Therefore,

$$v_z(r) = \left(\frac{1}{2k}\frac{dp}{dz}\right)^{1/n} \frac{n}{1+n}\left(r^{(1+n)/n} - a^{(1+n)/n}\right). \tag{9.142}$$

For $n=1$, we recover the result for Newtonian flows [Eq. (9.45)], as we should. Clearly, the volumetric flow rate Q can be computed and, hence, so too the wall shear stress in terms of Q.

For example,

$$Q = \frac{\pi n}{1+3n}\left[\frac{a^{1+3n}}{2k}\left(-\frac{dp}{dz}\right)\right]^{1/n}. \tag{9.143}$$

Noting that Eq. (9.142) can be written as

$$v_z(r) = -\frac{n}{1+n}\left(\frac{a^{1+n}}{2k}\frac{dp}{dz}\right)^{1/n}\left(1 - \left(\frac{r}{a}\right)^{(1+n)/n}\right), \tag{9.144}$$

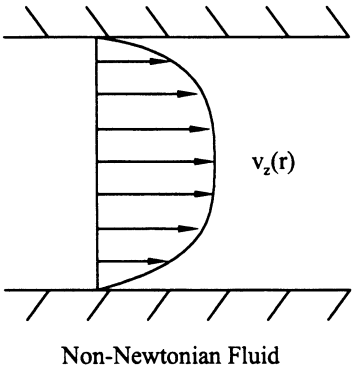

FIGURE 9.22 Non-Newtonian velocity profiles; note the more blunted profile than for the Newtonian case (cf. Fig. 9.13).

the maximum velocity is

$$v_z)_{\max} = v_z(r=0) = -\frac{n}{1+n}\left(\frac{a^{1+n}}{2k}\frac{dp}{dz}\right)^{1/n}; \tag{9.145}$$

hence, we can write

$$\frac{v_z(r)}{v_z)_{\max}} = 1 - \left(\frac{r}{a}\right)^{(1+n)/n}, \tag{9.146}$$

which facilitates plotting the velocity profile. Figure 9.22 shows, for example, a profile for $n < 1$, which differs from the parabolic profile for $n = 1$. In particular, note the blunted profile for the pseudoplastic response, remembering from Chap. 7 that blood exhibits a pseudoplastic character.

Chapter Summary

The *Navier–Stokes equations* are arguably the most important equations in fluid mechanics and they find wide usage in biofluid mechanics as well. Although one must resort to the numerical solution (often via finite element methods; see Humphrey and Taylor 2008) of these coupled, nonlinear partial differential equations in many cases, there are a number of exact analytical solutions that are both useful and instructive. We thus strongly encourage the reader to understand well the solutions presented in Sects. 9.1–9.5.

In particular, solution of the velocity, pressure, and shear stress fields for a pressure-driven flow of a Newtonian fluid (e.g., standard culture media) between rigid parallel plates (Sect. 9.1) is especially important in endothelial cell *mechanobiology*, in which one seeks to correlate altered gene expression or signal pathway activity with shear stress. Similar solutions for pressure-driven

steady (Sects. 9.2 and 9.4) and unsteady (Sect. 9.5) flows of a Newtonian fluid in a tube are especially important in studying problems in cardiology, pulmonology, and urology, to name a few medical specialties, and so too for the one solution of a non-Newtonian flow (Sect. 9.6) in a circular tube.

We emphasize, therefore, that such closed-form solutions are useful for understanding the biomechanics (e.g., in vivo situations) and for designing rigorously interpretable experiments (e.g., both for the mechanics and the mechanobiology), including the devices to be used. Moreover, understanding fluid responses in diverse "simple" situations as discussed in this chapter helps the reader to build considerable intuition that will prove useful when later trying to interpret results stemming from finite element solutions of the Navier–Stokes equations for complex domains.

Appendix 9: Biological Parameters

Fundamental to computations in mechanics is knowledge of geometry, material properties, and applied loads for the system of interest. Here, we list information of importance to hemodynamics and airflow mechanics.

TABLE A9.1 Values for blood pressure in humans in health and hypertension.

	Diastolic	Systolic
Normotensive	<85	<130
High	85–89	130–139
Hypertensive		
Stage 1	90–99	149–159
Stage 2	100–109	169–179
Stage 3	110–119	180–209
Stage 4	>120	>210

Source: From J. H. Laragh and B. M. Brener (1995) *Hypertension, Pathophysiology, Diagnosis, and Management*. Raven Press, New York

TABLE A9.2 Mean blood vessel characteristics (man).

Vessel	Lumen radius	Wall thickness	Pressure (mmHg)	CSA (cm^2)
Aorta	1.25 cm	2 mm	120/80	4.5
Artery	0.4 cm	1 mm	112/79	20
Arteriole	15 mm	20 μm	45/35	400
Capillary	6 μm	1 μm	30	4500
Venule	10 μm	2 μm	20	4000
Vein	0.25 cm	0.5 mm	15	40
Vena cava	1.5 cm	1.5 mm	10	18

Note: Pressure is given as systolic/diastolic if pulsatile; CSA is the accumulative cross-sectional area. Vena cava pressures fluctuate with pulmonary inspiration and expiration but are given as representative

Source: From Johnson (1991)

TABLE A9.3 Hemodynamic characteristics (man).

	α	$\overline{v}$ (cm/s)	Mean Re	Max Re
Ascending aorta	21	18	1,500	9,400
Abdominal aorta	12	14	640	3,600
Renal artery	4	40	700	1,300
Femoral artery	4	12	200	860
Inferior vena cava	17	21	1,400	3,000

Source: From Milnor (1989), p. 148

TABLE A9.4 Mean airway characteristics (man).

	Generation	Number	Diameter (mm)	Length (mm)	CSA (cm^2)	$\overline{v}$ (cm/s)	Re
Trachea	0	1	18	120	2.6	393	4,350
Main bronchus	1	2	12.2	47.6	2.3	427	3,210
Lobar bronchus	2	4	8.3	19.0	2.2	462	2,390
Lobar bronchus	3	8	5.6	7.6	2.0	507	1,720
Segmental Bronchus	4	16	4.5	12.7	2.6	392	1,110
Terminal Bronchus	11	2,050	1.09	3.9	19	52.3	34
Alveoli	Last	300×10^6	0.28	0.28	—	—	—

Note: CSA is the accumulative cross-sectional area
Source: From Weibel (1963)

TABLE A9.5 Ventilation–perfusion ratios.

	% Lung volume	Alveolar Q (cm^3/s)	Perfusion Q (cm^3/s)	Ventilation/perfusion ratio
Top	7	4	1.2	3.3
	8	5.5	3.2	1.8
	10	7.0	5.5	1.3
	11	8.7	8.3	1.0
	12	9.8	11.0	0.9
	13	11.2	13.8	0.8
	13	12.0	16.3	0.73
	13	13.0	19.2	0.68
Bottom	13	13.7	21.5	0.63
Total	100 %			

Source: From Johnson (1991), p. 178

TABLE A9.6 Density and viscosity for common fluids.

Material	Density (kg/m^3)		Viscosity (Ns/m^2)	
	20 °C	37 °C	20 °C	37 °C
Air	1.208	1.142	1.8×10^{-5}	2.0×10^{-5}
Water	998	995	1.0×10^{-3}	7.5×10^{-4}
Plasma	-	1020	1.9×10^{-3}	1.2×10^{-3}
Glycerin	1,260	-	1.6	0.45

Notes: The density of water @ 4 °C is 1,000 kg/m^3, which is used to compute specific gravities: $SG = \rho/\rho_{H_2O}$ at 4 °C. 1P = 0.1 N s/m^2 and thus 1 cP = 1×10^{-3}Ns/m^2. Finally, the viscosity tends to vary as $\mu \sim Ae^{B/T}$ for fluids, where A and B are material parameters, and T is temperature.

Exercises

9.1 Design (sketch) an experimental setup that ensures a constant steady flow within a parallel-plate device. Discuss various options with regard to how to generate the requisite constant pressure gradient.

9.2 The velocity profile in Eq. (9.15) represents a flow between parallel plates relative to an (o; x, y) coordinate system with the origin at the bottom plate. Show that the solution can alternatively be written as

$$v_x(y) = -\frac{1}{2\mu}\left(\frac{dp}{dx}\right)\left(\frac{h^2}{4} - y^2\right)$$

if the origin of the coordinate system is at the centerline (i.e., $y \in [-h/2, h/2]$). Show, too, that regardless of the particular coordinate system used, the values of Q and τ_w are the same for this Poiseuille flow.

9.3 To facilitate access to the cells, some researchers use a parallel flow setup in an incubator wherein the bottom plate is stationary but the top surface of the fluid is exposed to an air/CO_2 environment (i.e., a free surface). Assuming a steady, incompressible, fully developed, 1-D flow, show that

$$Q = -\frac{h^3 w}{3\mu}\left(\frac{dp}{dx}\right) \text{ and } \tau_w = \frac{3\mu Q}{wh^2}.$$

9.4 A constant-pressure gradient $dp/dx = 0.2$ kPa/m is used to drive *glycerin* through a parallel-plate device with gap $h \sim 0.2$ m. Find the maximum velocity and volumetric flow rate per unit width. Compare these values to those for water. Assume that the temperature is ~20 °C. Values for the viscosities are in Appendix 9.

9.5 Is the flow field in Example 9.2 irrotational?

9.6 Assuming a steady flow with no gravity, find the velocity in the x direction for the problem in Fig. 9.23, where U is constant and the fluid is at a constant pressure.

FIGURE 9.23

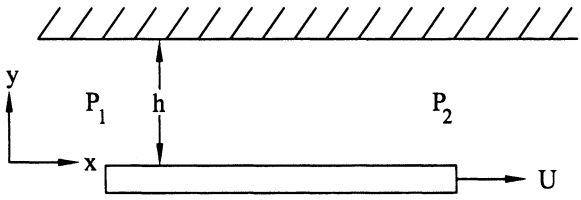

9.7 Solve for the flow between parallel plates (cf. Example 9.2) with both $dp/dx \neq 0$ (i.e., $p_1 > p_2$) and $U_0 \neq 0$. Calculate Q and $v_x)_{\max}$, as well as σ_{xy} and τ_w in terms of Q.

9.8 For the problem in Example 9.3, show that

$$Q = \frac{\rho g \sin\theta h^3}{3\mu}.$$

Furthermore, plot the velocity distribution $v_x/v_x)_{\max}$ on the abscissa versus the depth of the fluid (y/h) on the ordinate. Note that both variables are nondimensional and that they will vary from 0 to 1 regardless of the specific values in the problem. Finally, plot a normalized shear stress $\sigma_{xy}/\sigma_{xy})_{\max}$ versus y/h and discuss based on the shape of the velocity distribution curve.

9.9 A biomedical device is thrombogenic and thus must be coated with a thin biocompatible film as in Fig. 9.24. Assume that the fluid adheres to the device (no slip) as the device is pulled through it. Assume a constant film thickness h, and that the fluid behaves as Newtonian and incompressible. By solving Navier–Stokes, show that

$$h = \sqrt{\frac{2\mu U}{\rho g_x}}.$$

Hint: Assume $v_x(y = h) = 0$ in addition to the free-surface boundary condition $\partial v_x/\partial y\ (y = h) = 0$. What is implied by the latter condition?

FIGURE 9.24

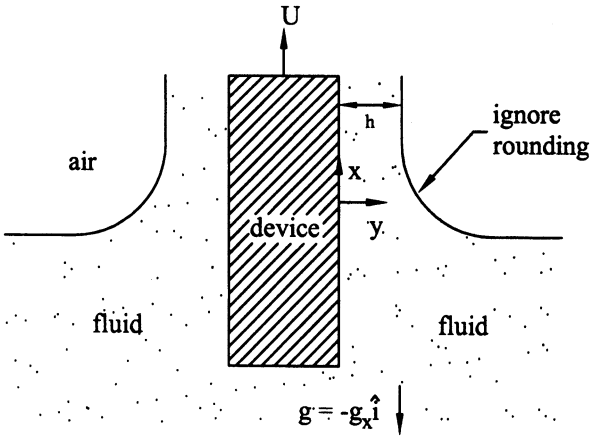

9.10 A plate with area A and mass M is sliding down an incline covered by a fluid film of constant thickness h (Fig. 9.25). (a) Determine the velocity profile in the fluid. (b) Determine the velocity of the plate U. Hint: Assume that the pressure gradient in the x direction is zero. Draw a free-body diagram of the plate and sum the forces to find an expression for the shear stress acting on the plate in terms of M, A, and g.

FIGURE 9.25

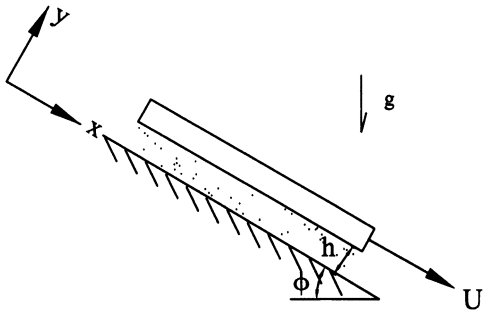

9.11 A rigid membrane with negligible thickness is located between two belts and is free to move (Fig. 9.26). The top belt is moving to the right with velocity $2\,U$. The bottom belt is moving to the left with velocity U. The fluid in section 1 (lower-half) has viscosity μ_1 and the fluid in section 2 (upper-half) has viscosity μ_2, with $\mu_1 = 3\,\mu_2$. (a) Determine the velocity field in sections 1 and 2. (b) Determine the velocity of the membrane using the given coordinate system. Hint: Draw a free-body diagram of the membrane to find the boundary condition at $y = h$.

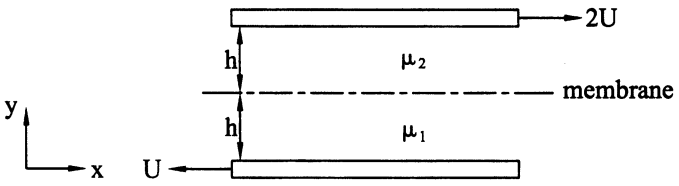

FIGURE 9.26

9.12 A fluid film of constant thickness h is sliding down a vertical wall (Fig. 9.27). Show that the velocity field is given by

$$v_y = \frac{\rho g h^2}{\mu}\left[\frac{x}{h} - \frac{1}{2}\left(\frac{x}{h}\right)^2\right]$$

for $x \in [0, h]$. Hint: Assume no-slip at the wall ($x = 0$) and assume that the shear stress due to the airflow over the fluid is negligible (i.e., $\partial v_y/\partial x|_{x=h} = 0$). Show that the velocity field is equivalent to that obtained in Example 9.3 if $\theta = 90°$.

FIGURE 9.27

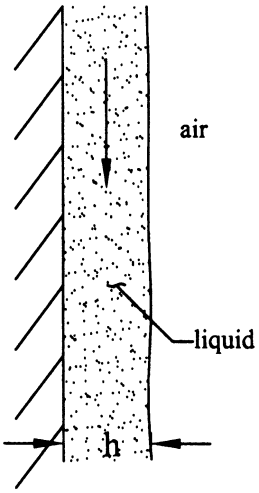

9.13 Show that the governing differential equation [Eq. (9.39)] for a steady flow of a Newtonian fluid in a rigid circular tube can be written as

$$\frac{1}{\mu}\frac{dp}{dz} = \frac{d^2 v_2}{dr^2} + \frac{1}{r}\frac{dv_z}{dr}.$$

Consequently, the equation can be solved by assuming a solution of the form $v_z \propto r^n$. Show that the solution is the same as that in Eq. (9.45).

9.14 Ex vivo perfusion systems are becoming more common in vascular research. Assuming a fully developed laminar flow, the wall shear stress in the perfused vessel is estimated by

$$\tau_w = \frac{4\mu Q}{\pi r_i^3}.$$

If $r_i \sim 2.2$ mm (porcine carotid) and $\mu = 4$ cP (Han and Ku 2001) find the value of Q necessary to produce a physiologic wall shear stress ~1.5 Pa.

9.15 Estimate the value of the Reynolds' number in the vena cava in a human. For comparison, note that for the vena cava of a dog, the diameter is ~1.25 cm, the mean velocity ~33 cm/s, the wall shear rate ~211 s^{-1}, the viscosity ~3 cP, and, thus, τ_w ~0.63 Pa. What is the associated value of the skin friction coefficient c_f?

9.16 Both in vivo and in vitro experiments show that the erythrocytes in blood vessels do not distribute themselves evenly across the cross section of a large blood vessel. Instead, they tend to accumulate along the centerline, thereby allowing, in a statistical sense, a thin cell-free layer to form along the wall of the vessel called the plasma layer (Fig. 9.28). Let the central core region containing cells have a viscosity μ_c and the cell-free plasma layer have a viscosity μ_p and thickness δ. In each region, assume that the flow is Newtonian. Use the Navier–Stokes equation to find (a) the velocity profile in the core region $v_z^c(r)$, (b) the velocity profile in the plasma layer $v_z^p(r)$, (c) the core volumetric flow rate Q_c, and (d) the plasma layer volumetric flow rate Q_p. Hint: Assume steady, unidirectional flow with a pressure gradient in the z direction to drive the flow. The velocity and shear stress in each region must be the same at the interface $r = a - \delta$.

FIGURE 9.28

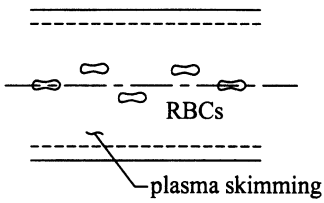

9.17 For a pressure-driven axial flow between long concentric cylinders (similar to that in Fig. 9.14 but for an axial flow; see Fig. 9.29), find the expression for the velocity profile in the z direction if the inner cylinder is of radius b and outer cylinder is of radius a. This problem relates to flow in an airway or blood vessel in which a central catheter has been placed. In particular, show that (Slattery 1981)

$$v_z(r) = \frac{-a^2}{4\mu}\left(\frac{dp}{dz}\right)\left(1 - \frac{r^2}{a^2} + \frac{1-\beta^2}{\ln(1/\beta)}\ln\frac{r}{a}\right),$$

where $b = \beta a$ and $\beta < 1$. In addition, find an expression for the volumetric flow rate Q. Note that $b = 0$ recovers Eq. (9.45).

FIGURE 9.29

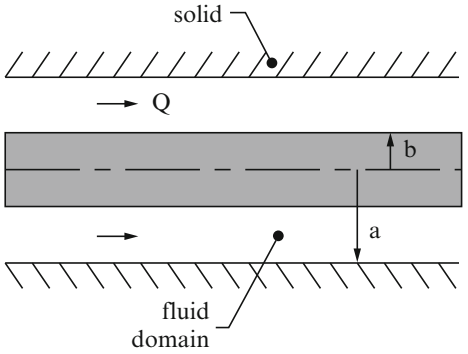

9.18 The viscosity in a concentric cylinder viscometer was shown to be calculated via

$$\mu = \frac{T(b^2 - a^2)}{4\pi\omega h a^2 b^2},$$

where T is the applied torque, a and b are the inner and outer radii, respectively, h is the height, and ω is the angular velocity. In contrast, a so-called capillary viscometer allows one to measure viscosity according to

$$\mu = \frac{-\pi a^4}{8Q}\left(\frac{dp}{dz}\right),$$

where dp/dz is the applied pressure gradient, a is the radius of the capillary (i.e., straight tube), and Q is the volumetric flow rate. Show that this equation is correct and state the associated restrictions that govern the experimental setup.

9.19 We have seen that there are many different types of viscometers, including the concentric-cylinder (Sect. 9.3) and the cone-and-plate (Sect. 7.6) devices. Explain how the results of Sect. 9.2 can be used to design a "capillary viscometer." Also discuss why, in contrast to the cone-and-plate viscometer, the capillary viscometer would not be useful for non-Newtonian fluids.

9.20 Similar to the previous exercise, explain how the results of Sect. 9.1 can be used to design a parallel-plate *flowmeter* to measure Q.

9.21 Synthecon, Inc. is a company that produces rotary cell culture systems, or *bioreactors*. According to literature on their website, a bioreactor is any device that monitors and controls the environment of a population of cells so as to promote normal metabolic and other activities. They write further that "the fluid-filled rotating wall vessel (RWV) bioreactor is a recently developed cell culture device that is able to successfully integrate cell–cell and cell–matrix co-localization and three-dimensional interaction with excellent low-shear mass-transfer of nutrients and wastes, without sacrificing one parameter for the other. Designed by Ray Schwarz, David Wolf, and Tinh Trinh at the Johnson Manned Spaceflight Center, the RWV bioreactor consists of a cylindrical growth chamber that contains an inner co-rotating cylinder with a gas exchange membrane." Write a three-page summary and critique of the NASA RWV bioreactor with particular emphasis on the fluid mechanics.

9.22 The velocity field for the NASA bioreactor (rotating cylinders) was assumed to be $\boldsymbol{v} = v_\theta(r)\hat{\boldsymbol{e}}_\theta$, with $v_\theta = r\omega$. This flow was shown to be "shearless" but not irrotational. How would the situation change if the angular velocity was a function of time [i.e., $\omega = \omega(t)$, with both cylinders still moving together]? Why? Is it possible to construct a Womersley-type solution for an oscillating case?

9.23 Confirm the result in Eq. (9.84) for the error in the inferred torques based on the exact versus flat plate approximations.

9.24 Let $b = a + h$ in Eq. (9.84). Show numerically how the error increases as the gap h increases. Hint: Consider different values of h as a percentage of a and plot the error versus h/a.

9.25 In some cases, the *pressure gradient* in a tube flow is computed as $-\partial p/\partial z = \Delta p/L$, where Δp is called the *pressure drop* ($\Delta p = p_i - p_o$, where subscripts i and o denote inlet and outlet) and L is the distance between the locations at which p_i and p_o are measured. If the straight tube is angled upward at angle α, show that the results from Sect. 9.2 hold provided that the pressure gradient is taken to be (Slattery 1981, p. 73)

$$-\frac{\partial p}{\partial z} = \frac{p_i - p_o - \rho g L \sin\alpha}{L}.$$

9.26 A catheter is to be coated by a nonthrombogenic film. A schema of the manufacturing setup is shown in Fig. 9.30. Assume that the flow is steady, laminar, and fully developed in the section L and that the coating fluid is Newtonian. Find the volumetric flow rate Q of the fluid through this section. Assuming the coating (film) thickness δ is uniform, find an expression for δ.

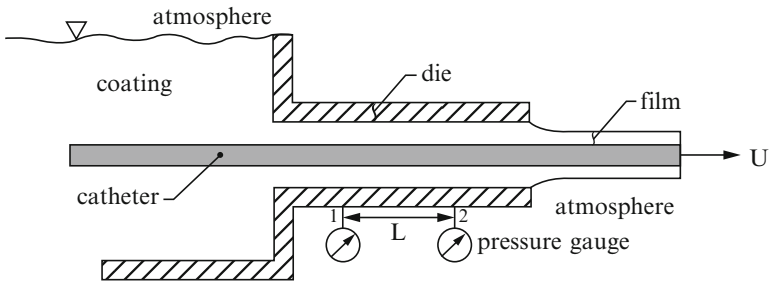

FIGURE 9.30

9.27 In Sect. 9.4, we found the solution to the flow in an elliptical cross section by assuming a form of $v_z(x, y)$ that satisfies the no-slip boundary condition exactly. Rederive the solution for steady, incompressible, fully developed, Newtonian flow in a rigid, straight, circular tube using this same idea. Hint: Let $v_z(r) = c(x^2 + y^2 - a^2) = c(r^2 - a^2)$.

9.28 We found that the velocity in an elliptical cross section is given by

$$v_z(x, y) = -\frac{1}{2\mu}\left(\frac{dp}{dz}\right)\frac{a^2b^2}{a^2 + b^2}\left(1 - \frac{x^2}{a^2} - \frac{y^2}{b^2}\right).$$

Show that, as reported by Zamir (2000), the volumetric flow rate and wall shear stress are given by

$$Q = -\frac{\pi a^3 b^3}{4\mu(a^2 + b^2)}\left(\frac{dp}{dz}\right)$$

and

$$\tau_w = \frac{dp}{dz}\left(\frac{a^2b^2}{a^2 + b^2}\right)\sqrt{\frac{x_1^2}{a^4} + \frac{y_1^2}{b^4}},$$

where (x_1, y_1), are points on the elliptical boundary.

9.29 The Fourier series representation for pressure in Eq. (9.97) can be written alternatively as

$$p(t) = p_m + \sum_{n=1}^{N} C_n \cos\left(\frac{2\pi nt}{T} + \Phi_n\right),$$

where T is the period (not temperature) and Φ_n is a phase shift. Prove that this is the case, and in so doing, relate the Fourier coefficients A_n and B_n to the amplitude C_n and the phase Φ_n. See Table 9.1.

9.30 Plot the function

$$f(t) = \sum_{n=1}^{N} C_n \cos\left(\frac{2\pi nt}{T} + \Phi_n\right)$$

given

C_n	7.5803	5.4124	1.5210	0.5217	0.8311
Φ_n	−173.9200	88.9220	−21.7046	−33.5370	−126.8100

Pick a constant value of $2\pi/T$ for a typical cardiac cycle.

9.31 Nagel et al. (J Clin Invest 94: 885–891, 1994) used a cone-and-plate device to subject cultured endothelial cells to various shear stresses. They showed that cultured human umbilical vein endothelial cells (HUVEC) exhibit time-dependent changes in the production of adhesion molecules for wall shear stresses τ_w from 0.25 to 4.6 Pa. They report that τ_w was given by

$$\tau_w = \frac{\mu\omega}{\alpha}\left[1 - 0.4743\left(\frac{r^2\omega\alpha^2\rho}{12\mu}\right)^2\right],$$

where μ is the viscosity of the culture media, ρ is its mass density, ω is the angular velocity of the cone, α is its inclination angle, and r is a radial distance from the symmetry axis. Show that the formula is approximately "correct."

9.32 Usami et al. (Ann Biomed Eng 21: 77–83, 1993) reported that a multidirectional steady-flow solution between parallel flat plates is given by

$$v_x = \frac{6}{h^2}z(h-z)\overline{v}_x(x,y), \quad v_y = \frac{6}{h^2}z(h-z)\overline{v}_y(x,y),$$

where h is the gap distance, z is the out-of-plane direction, and $\overline{v}_x$ and $\overline{v}_y$ are mean values over the gap at any (x, y). Show that in the case of $\overline{v}_x = c$, a constant, and $\overline{v}_y = 0$, one recovers the simple Poiseuille flow. Find the "value" of c. Show, too, that these results for $v_x(x_y\, y, z)$ and $v_y(x, y, z)$ are solutions to the incompressible Navier–Stokes equation and that

$$\tau_w \boldsymbol{n} = \tau_{13}\hat{\boldsymbol{e}}_1 + \tau_{23}\hat{\boldsymbol{e}}_2 = \frac{6\mu}{h}\overline{\boldsymbol{v}}.$$

Finally, note that this formulation allowed the design of a unique flow chamber, with particular advantages over the standard parallel-plate device.

9.33 Repeat the analysis in Sect. 9.6 for the flow of a power-law fluid between parallel plates. Let the gap distance be h and the width w and assume a fully developed, steady flow. If y $\in [-h/2, h/2]$, find the velocity distribution $v_x(y)$.

9.34 Plot the velocity distribution $v_x/v_{x)\max}$ in Exercise 9.33 versus depths y/h (ordinate) for $n = 0.8$, $n = 1$, and $n = 1.5$.

9.35 Plot Q(non-Newtonian)/Q(Newtonian) on the ordinate versus the power-law exponent n on the abscissa for n from 0.5 to 1.5 for the parallel-plate flow.

9.36 Given the following data for water

Temperature (°C)	Density (kg/m^3)	Viscosity (Ns/m^2)
4	1,000.00	1.568×10^{-3}
15	999.13	1.145×10^{-3}
20	998.00	1.009×10^{-3}
30	996.00	0.800×10^{-3}
40	992.00	0.653×10^{-3}

Use interpolation methods to find precisely $\rho(37\,^\circ\text{C})$ and $\mu(37\,^\circ\text{C})$. Given that $\mu = Ae^{B/T}$ (where T is the absolute temperature), find A and B for water.

9.37 A power-law (Ostwald-deWalle) model is given in Eq. (9.131) as

$$\sigma_{rz} = \kappa\left(\frac{\partial v_z}{\partial r}\right)^n,$$

where n is a parameter ($n > 1$ for dilatant and $n < 1$ for pseudoplastic) and κ is related to the "apparent" viscosity. Actually, it was proposed that the viscosity varied with the shear rate, namely

$$\sigma_{rz} = \mu(\text{shear rate})\frac{\partial v_z}{\partial r},$$

where the viscosity was found from experiments to be given by

$$\mu(\text{shear rate}) \sim \mu_a\left(\frac{\partial v_z}{\partial r}\right)^{n-1},$$

which recovers a Newtonian behavior if $n = 1$. A similar but different model (Hermes and Fredrickson) is of the form (Slattery 1981, p. 53)

$$\mu \sim \frac{m\mu_0}{m + \mu_0(\partial v_z/\partial r)^{1-n}},$$

where m, n, and μ_0 are parameters. Repeat the analysis in Sect. 9.6 using this model.

9.38 If we denote an arbitrary shear rate (e.g., $\partial v_z/\partial r$ or $\partial v_\theta/\partial r$) via the symbol γ then the viscosity for the power-law model is

$$\mu = \mu_a \gamma^{n-1}.$$

Hence,

$$\ln \mu = \ln \mu_a + (n-1)\ln \gamma$$

can be interpreted as a straight line $y = b + mx$. Use a linear regression method to compute μ_a and n for the data in Exercise 7.27 of Chap. 7.

9.39 The cross-sectional area A of an artery tends to taper exponentially as a function of distance from the heart. In particular, it has been shown in canines that

$$A = \pi a_0 e^{(-Bx/a_0)}$$

where a_0 is the radius at an upstream site, x is a distance along the aorta from that site, and $B \sim 0.02$–0.05. Plot the change in cross-sectional area for different values of B over a length of 20 cm.

9.40 For the solution of a flow down an inclined surface (Example 9.3), show that the maximum velocity occurs at the free surface, where

$$v_x)_{\max} = \frac{\rho g \sin\theta h^2}{2\mu}$$

and the volumetric flow rate is

$$Q = \frac{\rho g \sin\theta h^3 w}{3\mu}.$$

Also find the wall shear stress τ_w (at $y = 0$).

9.41 We have used the no-slip boundary condition at all solid–fluid interfaces (i.e., the fluid has the same velocity as the solid it contacts). This is clearly an approximation. Consider therefore, a *slip* boundary condition whereby

$$v_{\text{surface}} = \gamma \tau_w,$$

where γ is an empirical coefficient ($\gamma = 0$ for no-slip and a stationary surface). In the case of parallel-plate flow, with the coordinate system at the centerline,

$$v_{\text{surface}} \equiv v_x\left(y = \pm\frac{h}{2}\right) = \gamma\left[-\sigma_{yx}\left(\frac{h}{2}\right)\right] = -\gamma\frac{\partial v_x}{\partial y}\left(\frac{h}{2}\right).$$

Show that, in this case,

$$v_x(y) = c\left(1 - \frac{y^2}{h^2/4 - \gamma\mu h}\right),$$

where c can be written in terms of the volumetric flow rate or the pressure gradient. Hint: Use the condition that the velocity field is symmetric, $\partial v_x/\partial y = 0$ at $y = 0$. Note that if $\gamma = 0$, then we should recover our previous answer.

9.42 Equation (9.49) provides a relationship between the volumetric flow rate Q and the pressure gradient dp/dz for a rigid circular tube. The ratio of $|dp/dz|$ to Q provides a measure of the resistance to flow, which for the circular tube is $8\mu/\pi a^4$, which is to say, the resistance decreases as the luminal radius increases (to the fourth power). Similarly, find the ratio of $|dp/dz|$ to Q for flow in an elliptical tube [cf. Eq. (9.96)]. Compare the resistance to flow for these two geometries given the same cross-sectional area A.

9.43 Show that the velocity profile for a power-law fluid flowing between two parallel flat plates is given by (with the coordinate system centered between the plates with no-slip boundary conditions at $y = \pm h/2$)

$$v_x(y) = \frac{n}{1+n}\left(\frac{1}{k}\frac{dp}{dx}\right)^{1/n}\left(y^{1+1/n} - \left(\frac{h}{2}\right)^{1+1/n}\right)$$

and, consequently, that

$$Q = \left(-\frac{2nw}{2n+1}\right)\left(\frac{1}{k}\frac{dp}{dx}\right)^{1/n}\left(\frac{h}{2}\right)^{2+1/n}.$$

9.44 For Exercise 9.43, show that

$$v_x(y) = v_x)_{\max}\left[1 - \left(\frac{2y}{h}\right)^{1+1/n}\right].$$

Plot the velocity profile, normalized by $v_x)_{\max}$, for various values of n.

9.45 Solve Exercise 3.8 in Ethier and Simmons (2007), namely: "The binding strength of a single αIIbβ3 integrin complex to fibrinogen has been measured to be 60 to 150 pN. Suppose that a value of 100 pN is typical

for all integrins. How many integrin complexes would be required to maintain adherence of a vascular endothelial cell to the wall of a 8 mm diameter artery carrying 1.4 l/min of blood. You may treat the blood flow as steady, take blood viscosity to be 3.5 cP, and assume that the apical surface area of a single endothelial cell is 550 μm^2.

9.46 We close this chapter by emphasizing that the continuum assumption is expected to hold when $\delta/L << 1$, with δ a characteristic length scale of the microstructure and L a characteristic length scale of the physical problem. Hence, one would expect (cf. Table 9.1) the continuum assumption to hold for blood flow in the human aorta (dia ~ 2.5 cm, thus L on the order of centimeters) but not a capillary (dia ~ 10 μm, thus L on the order of microns), each relative to a red blood cell diameter of ~ 8 μm (and thus δ on the order of microns). Fahraeus and Lindqvist observed in 1931, however, that one must be thoughtful when using a continuum approach for blood vessels up to 1 mm in diameter. That is, they reported that the "effective viscosity" of blood in a continuum sense decreases as the diameter of the tube decreases. Discuss this "Fahraeus-Lindqvist" effect in a 2-page report in terms of "plasma skimming" as well as differential hydrodynamic forces that exist on deformable particles in a flow field. Both of these effects remind us of the need for diverse continuum theories, including the need for materially non-uniform (e.g., mixture) theories. Hint: also see Exercise 9.16.